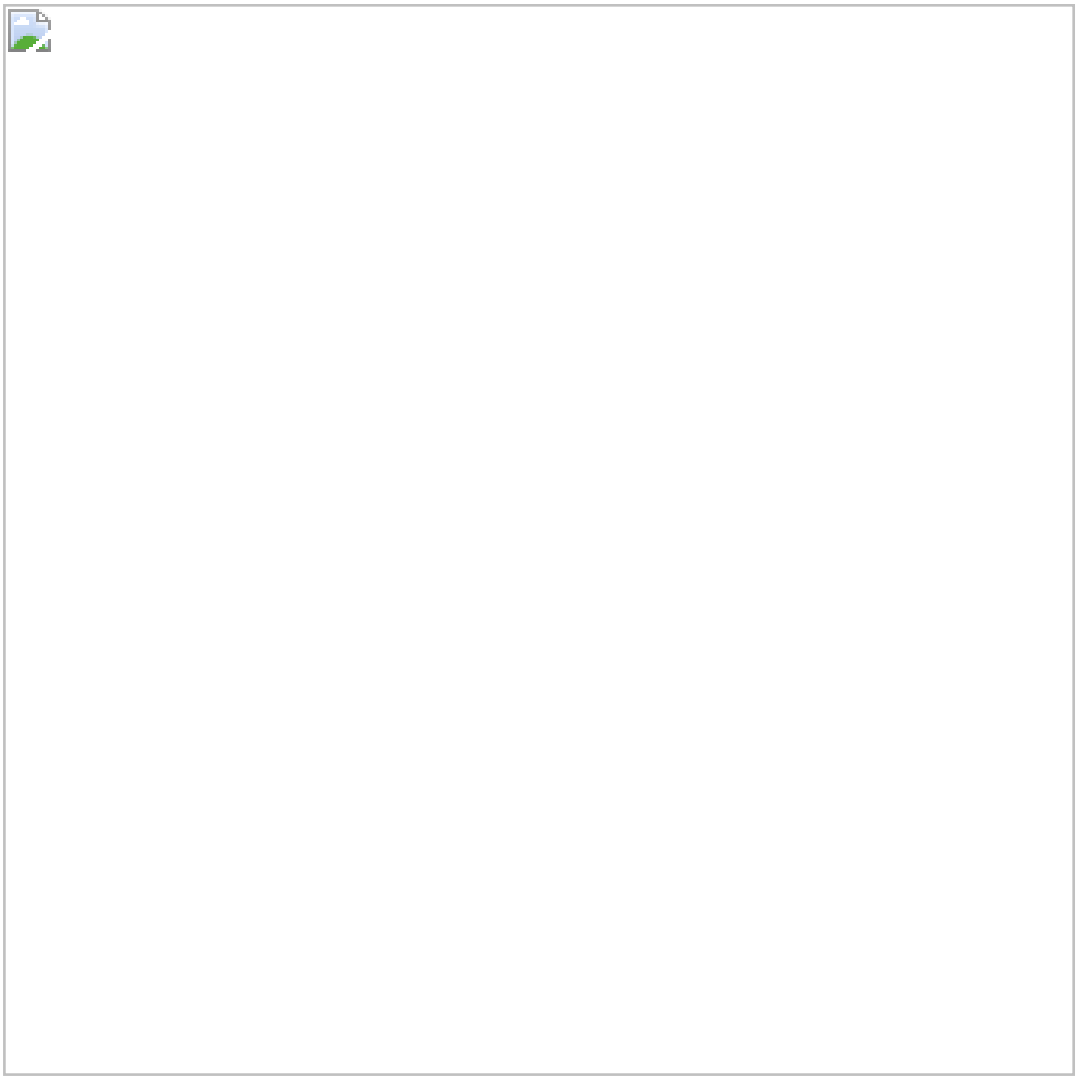

Decadal-Scale Variations in Glacier Area Changes Across the Southern Patagonian Icefield Since the 1970s

Authors: White, A., and Copland, L.

Source: Arctic, Antarctic, and Alpine Research, 47(1) : 147-167

Published By: Institute of Arctic and Alpine Research (INSTAAR), University of Colorado

URL: https://doi.org/10.1657/AAAR0013-102

Arctic, Antarctic, and Alpine Research, Vol. 47, No. 1, 2015, pp. 147–167

Decadal-scale variations in glacier area changes across the Southern Patagonian Icefield since the 1970s

A. White[1,2] *and*
L. Copland[1]

[1]Department of Geography, University of Ottawa, Room SMD 043, 60 University Pvt., Ottawa, Ontario, K1N 6N5, Canada
[2]Corresponding author:
awhit059@uottawa.ca

Abstract

A combination of Landsat and ASTER satellite scenes are used to quantify changes in the areal extent of glaciers in 130 basins across the Southern Patagonian Icefield (SPI). There was extensive net overall loss, with a reduction in ice area of 542 km^2 (~4% of the SPI) between the late 1970s and 2008/2010. For glaciers measured within individual periods, average losses occurred at a rate of 3.24% decade^{-1} between 1976/1979 and 1984/1986, 2.04% decade^{-1} between 1984/1986 and 2000/2002, and 2.24% decade^{-1} between 2000/2002 and 2008/2010. This indicates sustained losses, but no evidence for a recent acceleration. Since the 1980s, glaciers located in the northwest part of the SPI experienced the highest mean annual loss rates at 2.9% decade^{-1}. Mean glacier elevation provides the only significant topographic control on glacier changes for all measurement periods, and glacier losses are consistent with recent warming and changes in precipitation observed for this region.

DOI: http://dx.doi.org/10.1657/AAAR0013-102

Introduction

The Southern Patagonian Icefield (SPI), also known as Hielo Patagónico Sur, is the largest temperate ice mass in the southern hemisphere. Straddling the Andes Mountains between Chile and Argentina, it is ~400 km long, averages ~50 km wide, had an area of ~13,000 km^2 in 2008 (this study), and rises to >3000 m above sea level (a.s.l.) (Fig. 1). The north-south orientation of the mountain range acts as an orographic barrier, resulting in high precipitation to the west and drier conditions on the lee side to the east (Carrasco et al., 2002; López et al., 2010). Maximum precipitation has been estimated at >8000 mm w.e. (water equivalent) a^{-1} on the western side of the icefield plateau, but this drops to only a few hundred mm w.e. a^{-1} on the eastern side (Rivera, 2004). The heavy precipitation along the west side of the icefield is related to marine influences, including persistent westerlies that bring frequent cyclones to the coast (Carrasco et al., 2002; López et al., 2010).

Outlet glaciers flow from the icefield in all directions, although the majority typically flow either westward into tidewater fjords or eastward into freshwater lakes. Ice thicknesses at the floating fronts of several SPI glaciers (Tyndall, Grey, Moreno, Pio XI, and Upsala) have been estimated to be 200 to 400 m (Nichols and Miller, 1952; Casassa, 1992; Warren, 1994; Warren and Rivera, 1994; Warren et al., 1995; Aniya, 1999). Previous studies have used airborne and satellite imagery to inventory both the characteristics of SPI outlet glaciers (Aniya et al., 1996), as well as examine changes in their area, elevation, length, and volume on both regional (Aniya et al., 1997; Aniya, 1999; Chen et al., 2007; López et al., 2010; Davies and Glasser, 2012) and sub-regional scales (Rivera and Casassa, 2004).

Over the long-term, Davies and Glasser (2012) reported that the SPI lost a total of 1643 km^2 between 1870 and 2011, equivalent to 11.4% of its total area, with an acceleration in losses since 1986. The studies published in the 1990s by Aniya and co-workers examined the retreat rates of 48 SPI outlet glaciers between 1944/1945 and 1986. Aniya et al. (1992) reported a general retreat, with Aniya (1999) stating that this comprised an areal loss of 202 km^2 and, excluding advancing and steady-state glaciers, an average retreat rate of 0.192 km^2 a^{-1}. Strongly contrasting behaviors were sometimes observed between glaciers at the same latitude on either side of the SPI divide. For example, the O'Higgins Glacier had the highest total retreat (11 km) of any glacier on the eastern side of the SPI between 1945 and 1976, whereas the adjacent Pio XI Glacier had the greatest advance (9 km) of any glacier on the western side of the icefield over the same period (Aniya et al., 1992). This strongly contrasting behavior is somewhat unique for mid-latitude glaciers, with Rivera et al. (1997a, 1997b) arguing that recent advances of Pio XI have been due to surging.

Based on thickness data for five glaciers, Aniya (1999) estimated overall thinning rates of 1–3 m a^{-1} in the ablation zone of the SPI from 1944/1945 to 1986, which would account for a total ice loss of 100–300 km^3 from the 2452 km^2 ablation area of the icefield over this period (excluding Pio XI and Perito Moreno Glaciers). When Aniya (1999) applied this thinning rate to the 7083 km^2 accumulation area, a total volume loss of 285–670 km^3 was calculated (6.9–16.3 km^3 a^{-1}) from the SPI between 1944/1945 and 1986. This compares to estimated losses for the SPI of 13.5 ± 0.8 km^3 a^{-1} over the period 1968/1975 to 2000, and losses of 38.7 km^3 a^{-1} over the period 1995–2000, based on a comparison of Shuttle Radar Topography Mission (SRTM) data with historical cartography (Rignot et al., 2003). More recently, Jacob et al. (2012) computed a mass loss rate of 23 ± 9 km^3 a^{-1} for the SPI from January 2003 to December 2010, based on data from the Gravity Recovery and Climate Experiment (GRACE).

In the southeastern part of the SPI, Rivera and Casassa (2004) compared digital elevation models (DEMs), global positioning system (GPS) data, and optical survey data to reveal an 8% total areal loss from 1945 to 2000, with strong thinning in the ablation zone of most glaciers from 1945 to 1995, but little evidence for change in their upper accumulation areas. Recent observations of thinning from 2000 to 2012 by Willis et al. (2012) indicate that losses now extend to the highest elevations for most of the SPI, and predominantly across the large eastern glaciers. The observed thinning and retreat over the past century has been linked to both atmospheric warming and glacier dynamics, in part due to high thinning rates causing an increase in the buoyancy of glacier tongues and resultant increase in flow rates and calving from longitudinal stretching (Rignot et al., 2003; Rivera and Casassa, 2004). The rate of retreat

1523-0430/13 $7.00

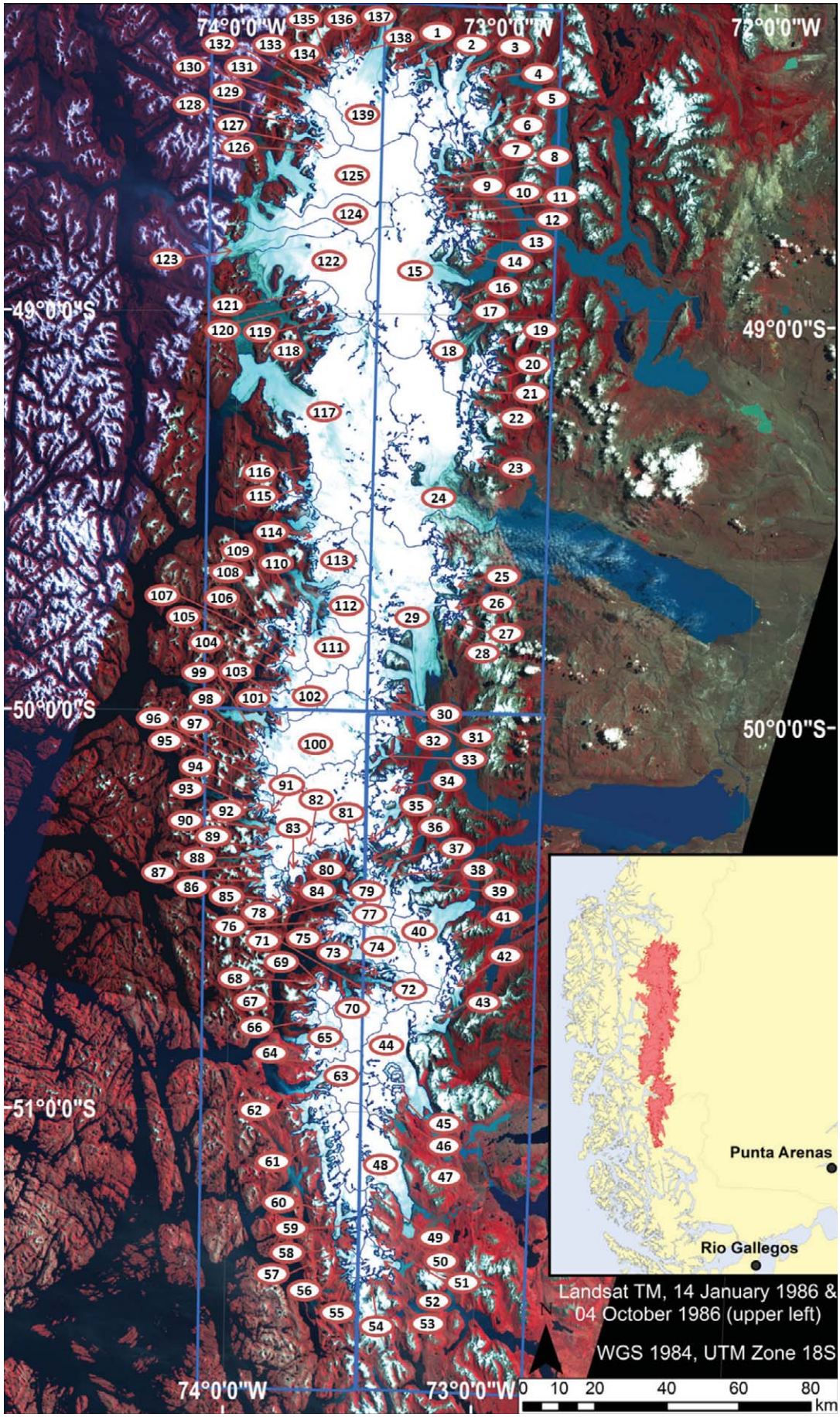

FIGURE 1. Landsat TM mosaic (14 Jan 1986 and 4 Oct 1986) of the Southern Patagonian Icefield (SPI) with the Glacier ID of the glaciers measured in this study (see Tables 2 and 3). Blue boxes indicate the quadrants used to separate the SPI into four substudy areas: northeast, southeast, southwest, and northwest.

may also be controlled by the presence of debris cover in the ablation area. For example, Rivera and Casassa (2004) found that surface thinning rates on the terminus of debris-covered Glaciar Frías averaged 3.2 ± 0.9 m a^{-1} between 1975 and 1998, but that surface thinning rates averaged 7.6 ± 0.9 m a^{-1} on nearby debris-free Glaciar Dickson over the same period.

The objective of this study is to quantify decadal changes in the extent of the ablation zone of individual glaciers across the SPI, and to understand the topographical and climatological factors that are influencing these changes. This builds on previous studies which have relied on measurements taken from only the largest glaciers (e.g., Aniya, 1999), or from the entire region at once (e.g., Rignot et al., 2003), which has limited the understanding of local variability. The recent inventory of Davies and Glasser (2012) addressed some of these issues by determining changes for the SPI over the periods 1870 to 1986, 1986 to 2001, and 2001 to 2011. Our study expands upon their coverage to include changes since the 1970s, and provides an independent quantification of area changes for both small and large glaciers. We also provide a detailed quantification of the connections between glacier physical characteristics and observed changes. Our analysis is focused on the SPI due to its dominance as the largest ice mass in this region.

Data and Methods

Changes in the area of the ablation zone for each glacier basin were determined from optical satellite imagery that fell within the periods 1976–1979, 1984–1986, 2000–2002, and 2008–2010 (Table 1). These periods were selected based on the availability of good quality satellite imagery; only nine glacier basins (accounting for ~61 km^2, or 0.5% of total glaciated area) were excluded from analysis due to lack of image data or the basin being too small to delineate accurately. Changes in the accumulation area were not analyzed due to the frequent presence of snow cover at high altitudes that made it impossible to accurately identify the outline of nunataks in this region. This approach is consistent with previous studies of the SPI, which have either not analyzed areal or thickness changes in the accumulation area (e.g., Aniya et al., 1992, 1997; Aniya, 1999; López et al., 2010), or have found little (Rignot et al., 2003; Rivera et al., 2005) to no significant change there (Rivera and Casassa, 2004). To analyze the spatial distribution of changes in glacier extent, the icefield was divided into quadrants (Fig. 1), chosen to capture the main climatological gradients of less precipitation from west to east, and warmer air temperatures from south to north.

BASIN BOUNDARIES

The SPI was initially divided into drainage basins provided by the Laboratoria de Glaciologia at the Centro de Estudios Científicos, Valdivia, Chile, as part of the Global Land Ice Measurements from Space (GLIMS) project. The delineation of these polygons was verified and updated against SRTM elevation data with a resolution of 3 arc seconds (~90 m), acquired from 11–22 February 2002. The elevation data was mainly used to help delineate basin boundaries in heavily snow covered areas, where it was difficult to define boundaries from optical imagery alone. The SRTM data were obtained from the United States Geological Survey (USGS), and a polygon shapefile was delineated for each drainage basin by using the Basin tool in ESRI ArcMap 9.3. To create the basins, sinks were filled, and a D8 flow model was used to determine flow direction.

GLACIER OUTLINES

An outline of the ablation area of each glacier basin was digitized from orthorectified Landsat satellite imagery for each of the four time periods: 1970s, 1980s, early 2000s, and late 2000s (Table 1). Images with minimal cloud cover from the summer and fall were preferentially chosen due to their minimum annual snow cover that facilitated clear delineation of glacier extents; no winter images were used in the analysis. The Landsat images acquired on 14 January 1986 (60 m resolution) provide a complete view of the SPI in one day and were mosaicked and used as the master image against which all other satellite imagery was georectified. Out of 45 Landsat scenes, only 3 were not aligned to this master mosaic within one pixel. These 3 scenes were georectified using 40 to 50 ground control points (GCPs) in ESRI ArcMap 9.3 and a third order polynomial transformation was applied. GCPs were chosen over flat, stable areas such as bedrock, and the final root mean square error (RMSE) for the 3 georectified scenes varied between 33.36 and 34.08 m (Table 1).

The Landsat imagery was viewed as a false color composite to delineate between ice and bedrock. Landsat Multispectral Scanner (MSS) scenes were represented with bands 8, 5, and 4 placed in the red, green, and blue (RGB) channels, respectively, while Landsat TM and ETM+ scenes were viewed with bands 7, 4, and 2 in the RGB channels. Other bands such as the thermal and 15 m panchromatic band (on the ETM+ sensor) were also used to refine the ice outlines. Due to a failure of the Landsat 7 scan line corrector, data gaps appear in the non-central parts of post-2003 ETM+ imagery as thin striping (NASA, 2009). In areas where this affected determination of a glacier outline, data gaps were filled by superimposing a Landsat scene with striping offset from the first scene, acquired within a year of the original. Two ASTER scenes were used in the analysis (Table 1), with their position verified against the 1986 Landsat mosaic using the methodology described above. The actual dates of image acquisition were used to convert measured area changes (km^2) into standardized rates of percentage change per decade. Most discussion and analysis focuses on these % $decade^{-1}$ changes, to avoid the bias of a few very large basins that dominate the km^2 changes. If more than one image was used to conduct a measurement, the date from the image with the greater spatial coverage was used.

The region of each glacier analyzed in this study consists of the lower portion which could be clearly delineated in all images of each basin. These outlines typically correspond to the ablation area, although they may not necessarily cover the entire ablation zone in situations where the snow cover occurred at low elevations in the imagery. The basin outline for any areas above this region were kept constant for all time periods and were based on the basin boundaries described in the Basin Boundaries section. A number of glaciers in the SPI have nunataks in their lower ablation areas that have become no longer surrounded by ice as their termini have retreated. In these cases the original nunatak area was subtracted from the ice area to prevent overestimation of ice loss.

All of the data concerning glacier areas were organized into a database by glacier ID number (Tables 2 and 3). Glacier names are listed where available, obtained from Aniya (1999), Zagier and Urruty (2010), and Chaltén Out Door maps (2010). The corresponding GLIMS glacier ID is also provided for each glacier, although in some instances multiple glacier basins identified in this study

TABLE 1

Satellite imagery used to measure glacier extents in this study. All images were obtained from the U.S. Geological Survey Global Visualization Viewer (http://glovis.usgs.gov/).

Image ID[a]	Sensor	Date	Image name	Level[b]	Resolution	SPI coverage	Number of GCPs	RMSE (m)
A1	Landsat 2 MSS	25 Feb 1976	LM22480941976056AAA05	L1T	60 m	Northern	50	33.36
A2	Landsat 2 MSS	04 May 1978	LM32460961978124AAA05	L1T	60 m	Southeast	—	—
A3	Landsat 2 MSS	02 Jan 1979	LM22460951979002AAA08	L1T	60 m	Moreno	—	—
A4	Landsat 2 MSS	02 Jan 1979	LM22460961979002AAA04	L1T	60 m	Southeast	—	—
A5	Landsat 2 MSS	22 Jan 1979	LM22480941979022AAA04	L1G	60 m	Northern	—	—
A6	Landsat 3 MSS	08 Mar 1979	LM32480941979067AAA03	L1G	60 m	Northern	40	34.08
A7	Landsat 3 MSS	08 Mar 1979	LM32480951979067AAA03	L1G	60 m	Central	—	—
B8	Landsat 5 MSS	26 Dec 1984	LM52310941984361AAA03	L1T	60 m	Northern	—	—
B9	Landsat 5 MSS	26 Dec 1984	LM52310951984361AAA03	L1T	60 m	Central	—	—
B10	Landsat 5 TM	27 Jan 1985	LT52310941985027AAA04	L1T	30 m	Northern	—	—
B11	Landsat 5 TM	27 Jan 1985	LT52310951985027AAA03	L1T	30 m	Central	—	—
B12	Landsat 5 MSS	14 Jan 1986	LM52310941986014AAA03	L1T	60 m	Northern	—	—
B13	Landsat 5 MSS	14 Jan 1986	LM52310951986014AAA03	L1T	60 m	Central	—	—
B14	Landsat 5 MSS	14 Jan 1986	LM52310961986014AAA03	L1T	60 m	Southern	—	—
B15	Landsat 5 TM	27 Sep 1986	LT52310941986270AAA11	L1T	30 m	Northern	—	—
B16	Landsat 5 TM	04 Oct 1986	LT52320941986277XXX02	L1T	30 m	Northern	—	—
B17	Landsat 5 TM	04 Oct 1986	LT52320951986277XXX02	L1T	30 m	Central-west	—	—
B18	Landsat 5 MSS	09 Feb 1987	LM52320941987040AAA03	L1T	60 m	Northern	43	33.89
C19	Landsat 7 ETM+	01 Mar 2000	LE72310952000061AGS00	L1T	30 m	Central	—	—
C20	Landsat 7 ETM+	27 Oct 2000	LE72310952000301EDC00	L1T	30 m	Central	—	—
C21	Landsat 7 ETM+	27 Oct 2000	LE72310962000301EDC00	L1T	30 m	Southern	—	—
C22	Landsat 7 ETM+	20 Mar 2001	LE72310942001079EDC02	L1T	30 m	Northern	—	—
C23	Landsat 7 ETM+	20 Mar 2001	LE72310952001079EDC02	L1T	30 m	Central	—	—
C24	Landsat 7 ETM+	07 May 2001	LE72310952001127EDC00	L1T	30 m	Central	—	—
C25	Landsat 7 ETM+	07 May 2001	LE72310962001127EDC00	L1T	30 m	Southern	—	—
C26	Landsat 7 ETM+	14 Oct 2001	LE72310942001287EDC00	L1T	30 m	Northern	—	—
C27	Landsat 7 ETM+	18 Jan 2002	LE72310942002018EDC00	L1T	30 m	Northern	—	—
C28	Landsat 7 ETM+	18 Jan 2002	LE72310952002018EDC00	L1T	30 m	Central	—	—
C29	Landsat 7 ETM+	08 Apr 2002	LE72310952002098EDC00	L1T	30 m	Central	—	—
C30	Landsat 7 ETM+	17 May 2002	LE72320942002137EDC00	L1T	30 m	Northern	—	—
C31	Landsat 7 ETM+	11 Dec 2002	LE72320942002345PFS00	L1T	30 m	Northern	—	—
C32	Terra ASTER	20 Feb 2005	AST_L1A.003:2028179529	L1B	15 m	Southern	—	—
D33	Landsat 7 ETM+	19 Jan 2008	LE72310952008019EDC00	L1T	30 m	Central	—	—
D34	Landsat 7 ETM+	28 Jan 2008	LE72300962008028EDC00	L1T	30 m	Southern	—	—
D35	Landsat 7 ETM+	04 Feb 2008	LE72310942008035EDC00	L1T	30 m	Northern	—	—
D36	Landsat 7 ETM+	04 Dec 2008	LE72310952008339EDC00	L1T	30 m	Central	—	—
D37	Landsat 7 ETM+	12 Jan 2009	LE72320942009012EDC00	L1T	30 m	Northern	—	—
D38	Landsat 7 ETM+	07 Dec 2009	LE72310942009341EDC00	L1T	30 m	Northern	—	—
D39	Landsat 7 ETM+	07 Dec 2009	LE72310952009341EDC00	L1T	30 m	Central	—	—

TABLE 1
Continued

Image ID[a]	Sensor	Date	Image name	Level[b]	Resolution	SPI coverage	Number of GCPs	RMSE (m)
D40	Landsat 7 ETM+	23 Dec 2009	LE72310962009357EDC00	L1T	30 m	Southern	—	—
D41	Landsat 7 ETM+	24 Jan 2010	LE72310942010024EDC00	L1T	30 m	Northern	—	—
D42	Landsat 7 ETM+	16 Feb 2010	LE72320942010047EDC00	L1T	30 m	Northern	—	—
D43	Landsat 7 ETM+	16 Feb 2010	LE72320952010047EDC00	L1T	30 m	Central-west	—	—
D44	Terra ASTER	16 Feb 2010	AST_L1A.003:2078231791	L1B	15 m	Central-west	—	—
D45	Landsat 7 ETM+	25 Feb 2010	LE72310952010056EDC00	L1T	30 m	Central	—	—
D46	Landsat 7 ETM+	04 Mar 2010	LE72320942010063EDC00	L1T	30 m	Northern	—	—
D47	Landsat 7 ETM+	29 Mar 2010	LE72310962010088EDC00	L1T	30 m	Southern	—	—
D48	Landsat 7 ETM+	16 May 2010	LE72310952010136EDC00	L1T	30 m	Central	—	—

[a] Image ID corresponds with Tables 2 and 3.
[b] Processing level: L1T = terrain corrected; L1G = systematically corrected; L1B = registered radiance at the sensor.

fell within one GLIMS glacier basin. Note that the basin outlines used in this study did not strictly follow GLIMS guidelines (e.g., as used by Davies and Glasser, 2012), as internal rock outcrops were not excluded from the glacier area measurements. This was due to the high number of nunataks, and the inability to precisely outline the nunataks through time due to fluctuating snow cover (Raup and Khalsa, 2010).

ERROR ANALYSIS

To calculate the uncertainty in the area change calculations due to satellite error we used the method outlined by Hall et al. (2003). First, the uncertainty of the change in terminus position in the linear dimension (d) between two satellite images was evaluated (after Williams et al., 1997):

$$d = \sqrt{r_1^2 + r_2^2} + RMSE, \quad (1)$$

where r_1 represents the cell size of the first image, r_2 the cell size of the second image, and RMSE the error determined during the georectification process (Table 1). To evaluate the worst-case value for uncertainty we used the largest cell size in our study for r_1 and r_2 (60 m), and the highest RMSE value (34.08 m) to produce a value for d of 118.93 m. To convert this linear uncertainty into an estimation of uncertainty in area change (a), we used (Hall et al., 2003):

$$a = A * (2d / x), \quad (2)$$

where $A = x^2$, and x = linear side dimension (60 m for MSS data). This produced a maximum uncertainty in area change of ±0.014 km^2 (due to satellite error), and considerably less than this for imagery with a resolution of 15 or 30 m.

To evaluate human error associated with digitizing the glacier extents, a blind-mapping study was completed by having the same operator independently digitize a small, medium, and large glacier five times for each time period, similar to the method of Paul et al. (2013). Glaciers #128 (2.33 km^2 in 1985), #6 (Melizo Sur; 33.80 km^2 in 1985), and #50 (Perito Moreno; 265.39 km^2 in 1985) were selected for this due to their range in area and distribution across the icefield. The mean error of all time periods varied between 0.0071 km^2 (0.30%) for #128, 0.0458 km^2 (0.14%) for Melizo Sur, and 0.0863 km^2 (0.03%) for Perito Moreno. The largest of these errors (0.0863 km^2) was summed with the satellite error (0.014 km^2) to provide a total error. In this study, glacier changes were therefore considered to be significant (beyond error limits) if >0.1 km^2.

Errors may also arise as a result of misinterpretation of the glacier extent due to factors such as snow or debris cover. To minimize the interference of snow cover during the delineation process, only images with minimal snow cover were used. Area change measurements were also only conducted for lower elevations, where snow cover is minimal. In the case of debris-covered glaciers, longitudinal surface structures visible on a debris-covered glacier surface (e.g., medial moraines) served as a guide for tracing the terminus (Glasser and Gudmundsson, 2012).

Results

Measured changes in the area of an ablation zone occurred due to changes in position of a glacier terminus, and/or narrowing of a glacier trunk and tributary branches. In general, there was a widespread decrease in extent for almost all glaciers over the period of study (Tables 2, 3, and 4; Figs. 2 and 3). From the 1970s to 1980s, out of 100 measured glaciers, 87 lost area, 2 experienced a gain, and 11 did not change beyond error limits (and a further 30 were excluded from analysis due to lack of cloud-free imagery) (Fig. 3, part a). From 1984/1986 to 2000/2002, 98 out of 130 glaciers lost area and 7 showed advance (Fig. 3, part b), while from 2000/2002 to 2008/2010, 83 out of 130 glaciers lost area and 3 expanded (Fig. 3, part c).

GLACIER CHANGES OF THE EASTERN SPI

A total of 52 glacier basins were measured on the eastern side of the SPI (Table 2). From the 1970s to the late 2000s, 49 of these glaciers experienced losses and 3 experienced no significant change.

TABLE 2

Variation in area of the ablation zone for the 52 glacier basins measured on the eastern side of the Southern Patagonian Icefield (SPI). Glacier ID # 31 was excluded from analysis due to lack of cloud-free imagery. Image ID indicates satellite images and dates used for each measurement period, as listed in Table 1. NSC = No significant change beyond error limit of 0.1 km2. Numbers in bold indicate area increase.

				Area change				
Glacier ID (Fig. 1)	Latitude/ Longitude	Glacier name (where available)/ GLIMS ID	Image ID (Table 1)	1984/1986 area (km^2)	1976/1979 to 1984/1986 (km^2) (*% decade^{-1}*)	1984/1986 to 2000/2002 (km^2) (*% decade^{-1}*)	2000/2002 to 2008/2010 (km^2) (*% decade^{-1}*)	Total: 1976/1979 to 2008/2010 (km^2) (%)
1	48°22.666′S, 73°25.344′W	G286499E48466S	A1, B12, C27, D46	6.61	–0.22 *(–4.68)*	–0.41 *(–3.90)*	–0.15 *(–3.02)*	–0.79 *(–11.50)*
2	48°22.580′S, 73°17.974′W	Lucia/ G286690E48460S	A1, B12, C31, D46	190.88	–1.02 *(–0.54)*	–8.88 *(–2.75)*	–1.36 *(–1.03)*	–11.26 *(–5.87)*
3	48°23.832′S, 73°10.010′W	Pascua/ G286840E48420S	A1, B12, C27, D42	112.39	–0.51 *(–0.45)*	–4.83 *(–2.68)*	–1.50 *(–1.72)*	–6.84 *(–6.06)*
4	48°25.151′S, 73°05.506′W	G286840E48420S	A1, B12, C27, D37	26.51	–0.47 *(–1.77)*	–0.71 *(–1.68)*	–0.36 *(–2.01)*	–1.55 *(–5.73)*
5	48°30.354′S, 73°04.049′W	Oriental/ G286937E48521S	A5, B10, C27, D42	73.68	–0.47 *(–1.05)*	–1.12 *(–0.90)*	–0.56 *(–0.95)*	–2.15 *(–2.90)*
6	48°35.198′S, 73°08.925′W	Melizo Sur/ G286829E48560S	A1, B10, C27, D42	33.80	–0.27 *(–1.33)*	–0.54 *(–0.93)*	–0.10 *(–0.38)*	–0.91 *(–2.66)*
7	48°36.725′S, 73°10.460′W	G286716E48597S	A1, B10, C27, D37	6.47	NSC	NSC	NSC	–0.11 *(–1.75)*
8	48°37.650′S, 73°14.382′W	Bravo/ G286716E48597S	A6, B10, C31, D42	135.53	–0.78 *(–0.97)*	–1.97 *(–0.81)*	–1.53 *(–1.60)*	–4.28 *(–3.14)*
9	48°40.778′S, 73°16.542′W	G286737E48704S	A6, B10, C27, D42	8.33	–0.20 *(–4.06)*	**0.14 *(1.00)***	NSC	–0.15 *(–1.74)*
10	48°42.603′S, 73°14.644′W	G286737E48704S	A1, B10, C31, D42	12.95	–0.87 *(–7.08)*	–0.24 *(–1.02)*	–0.19 *(–2.10)*	–1.30 *(–9.42)*
11	48°44.982′S, 73°13.401′W	G286746E48750S	A6, B10, C31, D42	24.85	–0.65 *(–4.31)*	–0.30 *(–0.67)*	–0.49 *(–2.80)*	–1.44 *(–5.65)*
12	48°45.940′S, 73°09.256′W	G286837E48784S	A5, B10, C27, D46	13.47	–0.22 *(–2.63)*	–0.15 *(–0.68)*	–0.15 *(–1.41)*	–0.52 *(–3.83)*
13	48°47.954′S, 73°05.262′W	G286905E48809S	A1, B9, C27, D46	11.85	–0.12 *(–1.13)*	–0.26 *(–1.27)*	–0.17 *(–1.81)*	–0.55 *(–4.56)*
14	48°49.984′S, 73°08.187′W	G286865E48834S	A1, B9, C27, D46	18.47	–0.18 *(–1.08)*	–0.20 *(–0.63)*	–0.11 *(–0.72)*	–0.48 *(–2.59)*
15	48°53.877′S, 73°13.813′W	O'Higgins/ G286651E48942S	A6, B10, C22, D38	807.22	–7.27 *(–1.51)*	–5.56 *(–0.43)*	–2.21 *(–0.32)*	–15.03 *(–1.85)*
16	48°58.913′S, 73°09.700′W	Gaea/ G286794E48989S	A5, B8, C27, D46	29.50	–0.44 *(–2.44)*	–1.26 *(–2.51)*	–0.49 *(–2.13)*	–2.19 *(–7.32)*
17	49°01.318′S, 73°10.147′W	G286847E49079S	A1, B10, C27, D35	6.93	–0.14 *(–2.23)*	NSC	NSC	–0.17 *(–2.37)*
18	49°03.758′S, 73°06.846′W	Chico/ G286847E49079S	A1, B10, C22, D38	199.14	–2.13 *(–1.17)*	–2.56 *(–0.79)*	–1.59 *(–0.92)*	–6.27 *(–3.11)*
19	49°06.118′S, 73°02.277′W	Pantoja & Milodon/ G287015E49071S	A1, B8, C27, D41	34.58	–0.95 *(–3.02)*	–0.48 *(–0.81)*	–0.10 *(–0.38)*	–1.53 *(–4.30)*
20	49°09.340′S, 73°01.857′W	Cagliero/ G287015E49071S	A1, B8, C27, D41	10.05	–0.11 *(–1.21)*	NSC	NSC	–0.12 *(–1.17)*
21	49°10.648′S, 73°05.462′W	Gorra Blanca (Sur)/ G286852E49174S	A1, B10, C27, D35	28.44	–0.54 *(–2.10)*	–0.60 *(–1.24)*	–0.18 *(–1.07)*	–1.32 *(–4.57)*
22	49°13.582′S, 73°06.960′W	Marconi/ G286875E49227S	A1, B10, C27, D38	21.44	–0.20 *(–1.03)*	–0.75 *(–2.06)*	–0.22 *(–1.32)*	–1.16 *(–5.38)*

TABLE 2

Continued

Glacier ID (Fig. 1)	Latitude/ Longitude	Glacier name (where available)/ GLIMS ID	Image ID (Table 1)	Area change				
				1984/1986 area (km^2)	1976/1979 to 1984/1986 (km^2) (*% decade^{-1}*)	1984/1986 to 2000/2002 (km^2) (*% decade^{-1}*)	2000/2002 to 2008/2010 (km^2) (*% decade^{-1}*)	Total: 1976/1979 to 2008/2010 (km^2) (%)
23	49°19.469′S, 73°03.361′W	De Quervain, Rio Tunel, Adela & Torre/ G286934E49316S	A5, B10, C27, D41	58.36	–0.50 *(–1.40)*	–1.79 *(–1.80)*	–0.20 *(–0.44)*	–2.48 *(–4.22)*
24	49°28.181′S, 73°09.247′W	Viedma/ G286731E49384S	A1, B10, C22, D41	1027.81	–4.27 *(–0.46)*	–7.82 *(–0.47)*	–5.78 *(–0.64)*	–17.87 *(–1.73)*
25	49°40.260′S, 73°08.494′W	Moyano/ G286639E49733S	A7, B11, C28, D45	93.90	–2.34 *(–4.13)*	–1.85 *(–1.16)*	–0.99 *(–1.33)*	–5.19 *(–5.39)*
26	49°43.525′S, 73°08.715′W	G286852E49737S	A7, B11, C28, D39	13.55	–0.14 *(–1.69)*	NSC	NSC	NSC
27	49°44.339′S, 73°07.001′W	G286852E49737S	A7, B11, C28, D45	0.96	NSC	NSC	NSC	NSC
28	49°47.061′S, 73°09.962′W	G286830E49782S	A7, B11, C28, D45	22.79	–0.22 *(–1.62)*	–0.25 *(–0.65)*	–0.18 *(–0.98)*	–0.65 *(–2.83)*
29	49°53.618′S, 73°17.483′W	Upsala/ G286639E49733S	A7, B11, C24, D39	925.02	–15.12 (–2.73)	–35.25 *(–2.34)*	–21.47 *(–2.81)*	–71.84 *(–7.64)*
30	49°57.964′S, 73°24.119′W	G286601E50018S	A7, B11, C28, D39	13.19	–0.73 *(–8.94)*	–0.45 *(–1.99)*	NSC	–1.23 *(–8.82)*
32	50°02.470′S, 73°22.232′W	Agassiz/ G286601E50018S	A7, B11, C28, D39	52.61	–0.53 *(–1.70)*	–0.51 *(–0.57)*	–0.30 *(–0.72)*	–1.34 *(–2.51)*
33	50°06.531′S, 73°24.580′W	Onelli & Bolados/ G286546E50107S	A7, B11, C28, D45	76.15	–1.18 *(–2.59)*	–4.19 *(–3.24)*	–3.19 *(–5.46)*	–8.56 *(–11.07)*
34	50°14.698°S, 73°21.168′W	Spegazzini, Peineta & Heim/ G286574E50253S	A7, B11, C28, D45	172.62	–1.56 *(–1.52)*	–0.73 *(–0.25)*	–0.64 *(–0.46)*	–2.93 *(–1.68)*
35	50°19.425′S, 73°27.895′W	G286574E50253S	A7, B11, C28, D39	19.46	–0.31 *(–2.67)*	–0.22 *(–0.66)*	NSC	–0.58 *(2.93)*
36	50°22.906′S, 73°27.132′W	Aguilera/ G286508E50363S	B11, C28, D45	9.59	No data	NSC	NSC	NSC
37	50°23.677′S, 73°25.057′W	Lago Escondida/ G286508E50363S	A7, B11, C28, D45	12.67	–0.37 *(–4.80)*	NSC	NSC	–0.47 *(–3.63)*
38	50°24.696′S, 73°22.422′W	Mayo/ G286621E50436S	A7, B11, C28, D45	42.14	–0.65 *(–2.56)*	–0.78 *(–1.09)*	–0.61 *(–1.82)*	–2.04 *(–4.76)*
39	50°25.558′S, 73°13.636′W	Ameghino/ G286701E50450S	A3, B11, C28, D45	101.91	–4.82 *(–7.43)*	–2.25 *(–1.30)*	–0.67 *(–0.82)*	–7.73 *(–7.24)*
40	50°30.222′S, 73°09.301′W	Perito Moreno/ G286789E50565S	A3, B11, C29, D45	265.39	–1.79 *(–1.10)*	–1.44 *(–0.31)*	**0.61** ***(0.29)***	–2.61 *(–0.98)*
41	50°34.401′S, 73°07.783′W	G286875E50590S	A4, B11, C19, D39	7.05	NSC	–0.41 *(–3.82)*	NSC	–0.47 *(–6.62)*
42	50°42.141′S, 73°06.116′W	Frias & Grande/ G286883E50681S	A4, B11, C28, D33	63.80	–3.42 *(–8.37)*	–2.75 *(–2.53)*	–1.71 *(–4.66)*	–7.87 *(–11.71)*
43	50°46.763′S, 73°11.324′W	Dickson/Cubo/ G286784E50766S	A4, B11, C29, D48	76.95	–4.83 *(–9.73)*	–6.18 *(–4.67)*	–1.43 *(–2.49)*	–12.44 *(–15.22)*
44	50°56.514′S, 73°15.498′W	Grey/ G286655E50857S	A4, B11, C23, D47	280.93	–2.18 *(–1.27)*	–8.87 *(–1.95)*	–3.97 *(–1.62)*	–15.02 *(–5.31)*
45	50°56.646′S, 73°19.520′W	G286612E50970S	A4, B14, C25, D34	2.79	–0.11 *(–5.45)*	NSC	NSC	–0.18 *(–6.35)*

TABLE 2
Continued

Glacier ID (Fig. 1)	Latitude/ Longitude	Glacier name (where available)/ GLIMS ID	Image ID (Table 1)	Area change				
				1984/1986 area (km^2)	1976/1979 to 1984/1986 (km^2) (*% decade^{-1}*)	1984/1986 to 2000/2002 (km^2) (*% decade^{-1}*)	2000/2002 to 2008/2010 (km^2) (*% decade^{-1}*)	Total: 1976/1979 to 2008/2010 (km^2) (%)
46	50°59.069′S, 73°21.985′W	Pingo/ G286612E50970S	A4, B14, C21, D47	61.74	–1.02 *(–2.32)*	–0.85 *(–0.93)*	–1.57 *(–2.74)*	–3.44 *(–5.48)*
47	51°01.931′S, 73°23.253′W	G286601E51028S	A4, B11, C25, D47	12.76	–0.53 *(–6.52)*	–0.45 *(–2.15)*	–0.21 *(–1.91)*	–1.18 *(–8.90)*
48	51°11.361′S, 73°18.398′W	Tyndall/ G286570E51112S	A4, B14, C21, D47	329.54	–5.48 *(–2.33)*	–10.37 *(–2.13)*	–12.34 *(–4.10)*	–28.20 *(–8.42)*
49	51°12.130′S, 73°25.390′W	G286574E51205S	A4, B14, C25, D47	13.15	–0.84 *(–8.55)*	–1.13 *(–5.59)*	–0.11 *(–1.04)*	–2.08 *(–14.86)*
50	51°14.751′S, 73°25.352′W	G286594E51286S	A4, B14, C25, D34	16.81	–1.22 *(–9.63)*	–0.74 *(–2.87)*	–1.28 *(–4.71)*	–3.24 *(–17.98)*
51	51°19.574′S, 73°22.840′W	G286594E51286S	A4, B14, C25, D47	11.27	–1.23 *(–14.01)*	–0.27 *(–1.56)*	–0.33 *(–3.33)*	–1.83 *(–14.62)*
52	51°22.516′S, 73°20.642′W	Balmaceda/ G286605E51373S	A2, B14, C25, D47	70.13	–1.37 *(–2.48)*	–3.09 *(–2.87)*	–2.81 *(–4.71)*	–7.27 *(–10.17)*
53	51°24.212′S, 73°21.041′W	G286642E51401S	A4, B14, C25, D47	9.67	NSC	–0.36 *(–2.46)*	NSC	–0.50 *(–5.14)*
			Total (km^2)	5677.81	–74.51	–123.63	–70.64	–269.35

No glaciers showed a net advance. The greatest area loss of 71.84 km^2 occurred from Upsala Glacier (#29), which retreated by ~8 km over this period and lost a total of 7.64% of its area (Fig. 4, part a). Relative to initial area, the greatest loss came from glacier #50, which lost 17.98%.

Broken down by period, 47 out of 51 glaciers measured between 1976/1979 and 1984/1986 decreased in area, with total losses of 74.51 km^2 (1.31%) at a mean per basin rate of 3.44% $decade^{-1}$ (Table 4). None expanded during this period. During this interval the highest loss rate occurred from glacier #51 at 14.0% $decade^{-1}$. Over the next period, 1984/1986 to 2000/2002, the east side of the SPI lost 123.63 km^2 (2.18%) in area, with 43 out of 52 measured glaciers contributing to this loss. Only one glacier expanded (#9), by a total of only 0.14 km^2. Retreat rates during the second period were approximately half of those during the first period, at an average per basin rate of 1.68% $decade^{-1}$. This is exemplified by the fact that the highest retreat rates in this period amounted to 5.59% $decade^{-1}$ at glacier #49 and 4.67% $decade^{-1}$ at Dickson/Cubo Glacier (#43), compared to 8.55% $decade^{-1}$ and 9.73% $decade^{-1}$, respectively, for the same glaciers between 1976/1979 and 1984/1986.

By the third period, 2000/2002 to 2008/2010, the average per basin rate of area loss remained similar to the previous period, at 2.00% $decade^{-1}$, with a total loss from the eastern SPI of 70.64 km^2 (1.24%) (Table 4). During this interval, 38 out of 52 glaciers lost area, 13 underwent no significant change, and only the Perito Moreno (#40) expanded. However, the 0.61 km^2 expansion at the Perito Moreno was insufficient to offset the total losses of 3.23 km^2 recorded there between 1976/1979 and 2000/2002 (Fig. 4, part b). The highest shrinkage rates were similar to the previous period, at 5.46% $decade^{-1}$ at the Onelli Glacier (#33) and 4.7% $decade^{-1}$ at the Frias (#42), #50, and Balmaceda (#52) glaciers.

GLACIER CHANGES OF THE WESTERN SPI

Area fluctuations for the 78 glaciers measured on the west side of the SPI (Table 3) were generally more variable than those on the east side. Over the longest measurement period (1976/1979 to 2008/2010 for 49 glaciers, 1984/1986 to 2008/2010 for 29 glaciers, Table 3), the west side of the icefield lost a total area of 272.70 km^2 (3.58%) (Table 4). These changes were dominated by losses from a few very large glaciers in the NW part of the SPI between 1976/1979 and 2008/2010, including 53.75 km^2 from the Jorge Montt Glacier (#139; Fig. 5, part a) and >20 km^2 each from the Greve (#122), Occidental (#123), Tempano (#124), and Bernardo (#125) glaciers. Compared to the 69 glaciers that retreated during this period, only 2 showed net advance and 7 did not change beyond error limits. The greatest advance occurred on the Pio XI Glacier, which increased in area by a total of 18.19 km^2 (1.43%) (Fig. 5, part b).

Of the 49 glaciers measured between 1976/1979 and 1984/1986, 39 lost area and 2 expanded (Table 3). Overall, the western SPI reduced in area by 46.94 km^2 (0.62%) during this period, at an average per basin rate of 3.00% $decade^{-1}$ (Table 4). The largest absolute area losses occurred from some of the largest glaciers, such as Tempano Glacier (#124), which lost 9.37 km^2. The largest relative losses occurred on some of the smallest glaciers, such as the 2.46 km^2 glacier #132, which lost area at a rate of 11.36% $decade^{-1}$. Between 1984/1986 and 2000/2002, the west side of the icefield declined in area by 156.27 km^2 (2.05%), representing the lowest average per basin rate of loss for this region

TABLE 3

Variation in area of the ablation zone for the 78 glacier basins measured on the western side of the SPI. Glaciers with ID # 68, 105, 107, 108, 126, 129, 137, and 138 were excluded from analysis due to lack of cloud-free imagery. Image ID indicates satellite images and dates used for each measurement period, as listed in Table 1. NSC = no significant change beyond error limit of 0.1 km². Numbers in bold indicate area increase.

					Area change			
Glacier ID (Fig. 1)	Latitude/ Longitude	Glacier name/ GLIMS ID	Image ID (Table 1)	1984/1986 area (km²)	1976/1979 to 1984/1986 (km²) (*% decade⁻¹*)	1984/1986 to 2000/2002 (km²) (*% decade⁻¹*)	2000/2002 to 2008/2010 (km²) (*% decade⁻¹*)	Total: 1976/1979 to 2008/2010 (km²) *(%)*
54	51°25.323′S, 73°27.493′W	G286516E51409S	A4, B14, C21, D47	11.06	–0.82 *(–9.84)*	NSC	–0.14 *(–1.40)*	–1.06 *(–8.88)*
55	51°25.349′S, 73°29.537′W	G286516E51409S	B14, C25, D47	3.77	No data	NSC	NSC	NSC*
56	51°24.210′S, 73°30.392′W	G286516E51409S	B14, C25, D47	14.02	No data	–0.46 *(–2.15)*	–0.22 *(–1.84)*	–0.68 *(–4.87)**
57	51°21.605,S, 73°31.651,W	Snowy/ G286501E51367S	A2, B14, C25, D47	22.03	–0.38 *(–2.23)*	–2.88 *(–8.53)*	–0.66 *(–3.87)*	–3.92 *(–17.50)*
58	51°20.190′S, 73°28.481′W	G286533E51313S	A2, B14, C25, D34	22.83	–0.48 *(–2.05)*	–0.53 *(–2.33)*	NSC	–1.06 *(–4.55)*
59	51°16.951′S, 73°30.067′W	G286533E51313S	A2, B14, C25, C32	5.04	NSC	NSC	–0.12 *(–6.51)*	–0.29 *(–5.67)*
60	51°16.604′S, 73°32.982′W	HPS41/ G286493E51240S	A2, B14, C25, D34	76.44	–0.60 *(–1.01)*	–2.67 *(–2.28)*	–4.60 *(–9.26)*	–7.87 *(–10.22)*
61	51°02.370′S, 73°38.700′W	HPS38/ G286405E51035S	B14, C21, D34	155.75	No data	–8.75 *(–3.80)*	–3.48 *(–3.26)*	–12.23 *(–7.85)**
62	50°59.493′S, 73°41.417′W	G286356E50989S	B11, C24, D40	59.25	No data	–5.70 *(–5.91)*	–2.84 *(–6.14)*	–8.54 *(–14.42)**
63	50°55.984′S, 73°39.240′W	Amalia/ G286466E50914S	B11, C28, D44	172.87	No data	–2.25 *(–0.77)*	–0.24 *(–0.18)*	–2.50 *(–1.44)**
64	50°52.814′S, 73°38.725′W	G286386E50824S	B11, C28, D44	2.74	No data	–0.17 *(–3.71)*	NSC	–0.24 *(–8.61)**
65	50°49.502′S, 73°42.000′W	Asia/ G286386E50824S	B11, C24, D44	127.96	No data	–2.73 *(–1.31)*	–0.17 *(–0.16)*	–2.91 *(–2.27)**
66	50°46.516′S, 73°40.772′W	G286359E50726S	B11, C20, D44	21.65	No data	–0.93 *(–2.72)*	–0.32 *(–1.67)*	–1.25 *(–5.78)**
67	50°43.897′S, 73°40.997′W	G286359E50726S	B11, C28, D45	20.88	No data	–1.30 *(–3.67)*	–0.48 *(–3.03)*	–1.78 *(–8.55)**
69	50°41.206′S, 73°34.984′W	G286359E50726S	B11, C28, D45	33.72	No data	–0.30 *(–0.52)*	–0.40 *(–1.49)*	–0.70 *(–2.08)**
70	50°43.264′S, 73°30.877′W	HPS34/ G286514E50763S	B11, C28, D45	163.75	No data	–0.44 *(–0.16)*	–0.40 *(–0.30)*	–0.84 *(–0.51)**
71	50°41.301′S, 73°25.019′W	G286588E50706S	B11, C28, D45	17.99	No data	**0.12 *(0.40)***	NSC	NSC*
72	50°41.313′S, 73°19.031′W	Calvo/ G286717E50700S	B11, C28, D45	113.22	No data	NSC	NSC	NSC*
73	50°38.276′S, 73°25.875′W	G286601E50641S	B11, C28, D45	22.62	No data	NSC	NSC	NSC*
74	50°36.718′S, 73°31.352′W	HPS31/ G286599E50592S	B11, C28, D45	161.55	No data	–0.46 *(–0.17)*	–0.10 *(–0.08)*	–0.57 *(–0.35)**
75	50°33.416′S, 73°36.222′W	G286420E50545S	B11, C28, D45	46.40	No data	–0.78 *(–0.99)*	–0.29 *(–0.79)*	–1.08 *(–2.32)**
76	50°31.538′S, 73°36.879′W	G286420E50545S	B11, C28, D45	14.66	No data	–0.47 *(–1.89)*	NSC	–0.55 *(–3.78)**
77	50°28.926′S, 73°32.446′W	HPS29/ G286531E50505S	B11, C20, D45	87.60	No data	–1.66 *(–1.20)*	NSC	–1.67 *(–1.91)**

TABLE 3

Continued

Glacier ID (Fig. 1)	Latitude/ Longitude	Glacier name/ GLIMS ID	Image ID (Table 1)	Area change				
				1984/1986 area (km^2)	1976/1979 to 1984/1986 (km^2) (*% decade^{-1}*)	1984/1986 to 2000/2002 (km^2) (*% decade^{-1}*)	2000/2002 to 2008/2010 (km^2) (*% decade^{-1}*)	Total: 1976/1979 to 2008/2010 (km^2) *(%)*
79	50°26.951′S, 73°30.455′W	HPS28/ G286524E50439S	B11, C28, D45	46.25	No data	–0.74 *(–0.94)*	NSC	–0.76 *(–1.64)**
80	50°24.741′S, 73°30.074′W		B11, C28, D45	16.92	No data	–0.57 *(–1.99)*	–0.17 *(–1.29)*	–0.74 *(–4.39)**
81	50°21.093′S, 73°31.288′W	HPS27/ G286508E50363S	B11, C28, D45	39.73	No data	–0.47 *(–0.70)*	–0.11 *(–0.34)*	–0.58 *(–1.45)**
82	50°20.624′S, 73°34.649′W	G286508E50363S	B11, C28, D45	26.20	No data	–0.27 *(–0.62)*	–0.60 *(–2.83)*	–0.87 *(–3.32)**
83	50°22.131′S, 73°43.350′W	G286265E50389S	B11, C28, D45	36.14	No data	–1.02 *(–1.66)*	–0.42 *(–1.47)*	–1.44 *(–3.98)**
84	50°25.237′S, 73°46.869′W	G286176E50441S	B11, C28, D39	8.05	No data	–0.34 *(–2.46)*	–0.11 *(–1.76)*	–0.44 *(–5.51)**
85	50°28.567′S, 73°47.384′W	G286176E50441S	B11, C20, D44	18.12	No data	–0.24 *(–0.84)*	–0.26 *(–1.59)*	–0.50 *(–2.78)**
86	50°25.976′S, 73°53.605′W	G286176E50441S	A7, B11, C28, D45	46.71	–1.04 *(–3.71)*	–2.86 *(–3.60)*	–0.85 *(–2.39)*	–4.75 *(–9.94)*
87	50°23.280′S, 73°52.468′W	G286176E50441S	B11, C28, D43	1.57	No data	NSC	NSC	NSC*
88	50°22.695′S, 73°51.482′W	G286262E50339S	B11, C28, D45	5.26	No data	–0.45 *(–5.00)*	NSC	–0.50 *(–9.49)**
89	50°21.202′S, 73°52.467′W	Guilardi/ G286262E50339S	A7, B17, C20, D43	176.98	NSC	–0.56 *(–0.23)*	–0.25 *(–0.15)*	–0.86 *(–0.48)*
90	50°17.900′S, 73°48.903′W	Europa/ G286350E50231S	A7, B11, C20, D39	408.68	–1.32 *(–0.54)*	NSC	NSC	–1.42 *(–0.35)*
91	50°15.684′S, 73°51.052′W	G286127E50185S	A7, B11, C28, D43	5.20	–0.19 *(–5.96)*	NSC	–0.11 *(–2.51)*	–0.29 *(–5.40)*
92	50°14.544′S, 73°52.126′W	G286127E50185S	A7, B13, C20, D39	12.10	–0.38 *(–4.46)*	–0.42 *(–2.37)*	NSC	–0.89 *(–7.15)*
93	50°14.405′S, 73°54.272′W	G286127E50185S	A7, B13, C24, D43	3.96	NSC	–0.11 *(–1.83)*	NSC	–0.12 *(–3.04)*
94	50°12.483′S, 73°53.818′W	G286127E50185S	A7, B11, C20, D43	14.05	NSC	NSC	NSC	NSC
95	50°10.391′S, 73°52.324′W	G286127E50185S	A7, B11, C28, D45	23.97	–0.35 *(–2.44)*	–0.70 *(–1.72)*	–0.15 *(–0.78)*	–1.20 *(–4.92)*
96	50°08.616′S, 73°53.907′W	G286127E50185S	A7, B11, C28, D45	21.26	–0.54 *(–4.20)*	–0.73 *(–2.02)*	–0.31 *(–1.89)*	–1.58 *(–7.27)*
97	50°06.833′S, 73°54.694′W	G286127E50185S	A7, B11, C28, D45	8.75	–0.22 *(–4.09)*	–0.32 *(–2.15)*	NSC	–0.57 *(–6.34)*
98	50°05.544′S, 73°53.580′W	G286127E50185S	A7, B11, C28, D45	5.26	–0.15 *(–4.76)*	NSC	NSC	–0.22 *(–4.01)*
99	50°03.632′S, 73°54.866′W	G286336E50073S	A7, B11, C28, D45	5.74	NSC	–0.29 *(–2.93)*	NSC	–0.44 *(–7.61)*
100	50°04.212′S, 73°51.972′W	Penguin/ G286336E50073S	A7, B11, C20, D43	468.24	–2.55 *(–0.92)*	**0.14** ***(0.02)***	NSC	–2.46 *(–0.52)*
101	50°01.091′S, 73°49.962′W	G286278E49958S	A7, B11, C28, D43	20.88	–0.42 *(–3.35)*	–0.46 *(–1.29)*	–0.19 *(–1.15)*	–1.07 *(–5.01)*
102	49°58.575′S, 73°50.915′W	HPS19/ G286278E49958S	A7, B11, C20, D45	173.95	–0.53 *(–0.52)*	NSC	NSC	–0.45 *(–0.26)*

TABLE 3
Continued

Glacier ID (Fig. 1)	Latitude/ Longitude	Glacier name/ GLIMS ID	Image ID (Table 1)	Area change				
				1984/1986 area (km^2)	1976/1979 to 1984/1986 (km^2) (*% decade^{-1}*)	1984/1986 to 2000/2002 (km^2) (*% decade^{-1}*)	2000/2002 to 2008/2010 (km^2) (*% decade^{-1}*)	Total: 1976/1979 to 2008/2010 (km^2) *(%)*
103	49°56.912′S, 73°50.756′W	G286278E49958S	A7, B11, C28, D36	10.01	NSC	NSC	NSC	–0.18 *(–1.78)*
104	49°53.145′S, 73°48.175′W	G286202E49896S	A7, B11, C28, D45	50.73	–0.92 *(–3.01)*	**0.12** ***(0.14)***	–0.60 *(–1.44)*	–1.39 *(–2.69)*
106	49°49.660′S, 73°46.581′W	G286239E49805S	A7, B13, C24, D43	67.19	–0.51 *(–1.11)*	–0.57 *(–0.55)*	NSC	–1.13 *(–1.67)*
109	49°46.308′S, 73°47.011′W	G286239E49805S	B11, C24, D45	42.68	No data	–1.32 *(–1.91)*	–0.76 *(–2.08)*	–2.08 *(–4.88)**
110	49°45.533′S, 73°43.280′W	G286239E49805S	A7, B11, C24, D39	17.22	–0.78 *(–7.32)*	**0.17** ***(0.60)***	NSC	–0.59 *(–3.29)*
111	49°47.033′S, 73°37.464′W	HPS15/ G286381E49840S	A7, B11, C23, D45	193.16	–0.30 *(–0.26)*	NSC	NSC	–0.23 *(–0.12)*
112	49°43.659′S, 73°37.609′W	HPS13/ G286453E49741S	A7, B11, C28, D43	143.19	–0.44 *(–0.52)*	–0.11 *(–0.04)*	NSC	–0.50 *(–0.34)*
113	49°36.630′S, 73°40.709′W	HPS12/ G286408E49615S	A7, B13, C28, D42	206.04	–1.83 *(–1.29)*	–8.99 *(–2.72)*	–6.14 *(–3.85)*	–16.96 *(–8.16)*
114	49°31.622′S, 73°44.576′W	HPS10/ G286305E49539S	A7, B11, C24, D42	98.96	–1.03 *(–1.59)*	–0.52 *(–0.33)*	–0.89 *(–1.03)*	–2.43 *(–2.43)*
115	49°25.726′S, 73°43.600′W	G286288E49425S	A6, B12, C31, D46	43.87	**0.47** ***(1.58)***	**2.68** ***(3.62)***	**0.60** ***(1.79)***	**3.76** ***(8.66)***
116	49°23.377′S, 73°42.808′W	G286288E49425S	A6, B8, C31, D42	3.30	NSC	NSC	NSC	–0.11 *(–3.36)*
117	49°09.109′S, 73°56.289′W	Pio XI/ G286372E49263S	A1, B12, C30, D46	1278.50	**4.70** ***(0.37)***	**8.64** ***(0.41)***	**4.85** ***(0.48)***	**18.19** ***(1.43)***
118	49°02.987′S, 73°42.266′W	HPS09/ G286389E49031S	A1, B8, C30, D42	59.09	–0.58 *(–1.10)*	–3.20 *(–3.11)*	–3.92 *(–9.04)*	–7.70 *(–12.91)*
119	48°59.996′S, 73°37.970′W	G286389E49031S	A1, B16, C31, D37	12.38	–0.94 *(–6.65)*	NSC	NSC	–1.02 *(–7.66)*
120	49°00.386′S, 73°41.021′W	HPS08/ G286312E48981S	A1, B12, C31, D46	50.80	–1.01 *(–1.96)*	–5.04 *(–5.86)*	–0.16 *(–0.49)*	–6.20 *(–11.97)*
121	48°57.357′S, 73°44.645′W	G286312E48981S	A1, B16, C31, D37	37.64	–0.59 *(–1.45)*	–1.60 *(–2.62)*	NSC	–2.27 *(–5.92)*
122	48°57.402′S, 73°52.072′W	Greve/ G286344E48904S	A1, B12, C26, D46	526.41	–5.19 *(–0.99)*	–18.59 *(–2.24)*	–8.42 *(–1.98)*	–32.20 *(–6.06)*
123	48°50.899′S, 74°01.084′W	Occidental/ G286139E48833S	A1, B16, C31, D42	185.26	–7.43 *(–3.63)*	–7.48 *(–2.49)*	–8.11 *(–6.34)*	–23.02 *(–11.95)*
124	48°43.151′S, 73°56.983′W	Tempano/ G286310E48760S	A1, B16, C31, D46	291.09	–9.37 *(–2.94)*	–7.33 *(–1.56)*	–3.84 *(–1.87)*	–20.55 *(–6.84)*
125	48°38.426′S, 73°51.050′W	Bernardo/ G286418E48657S	A1, B12, C27, D37	584.67	–3.01 *(–0.52)*	–20.02 *(–2.14)*	–5.26 *(–1.33)*	–28.28 *(–4.81)*
127	48°33.960′S, 73°47.298′W	G286248E48539S	A1, B15, C31, D37	68.42	–3.39 *(–4.46)*	–3.23 *(–2.91)*	–4.43 *(–11.16)*	–11.06 *(–15.40)*
128	48°31.130′S, 73°45.777′W	G286248E48539S	A1, B12, C27, D42	2.33	–0.20 *(–8.09)*	–0.20 *(–5.45)*	NSC	–0.44 *(–17.50)*
130	48°29.816′S, 73°45.520′W	G286248E48539S	A1, B12, C27, D37	7.84	–0.26 *(–3.29)*	–0.64 *(–5.12)*	–0.17 *(–3.47)*	–1.08 *(–13.34)*
131	48°27.136′S, 73°46.066′W	Ofhidro/ G286323E48495S	A1, B12, C22, D46	110.67	–0.85 *(–0.77)*	–3.06 *(–1.82)*	–2.29 *(–2.37)*	–6.19 *(–5.55)*

TABLE 3

Continued

Glacier ID (Fig. 1)	Latitude/ Longitude	Glacier name/ GLIMS ID	Image ID (Table 1)	Area change				
				1984/1986 area (km²)	1976/1979 to 1984/1986 (km²) (*% decade⁻¹*)	1984/1986 to 2000/2002 (km²) (*% decade⁻¹*)	2000/2002 to 2008/2010 (km²) (*% decade⁻¹*)	Total: 1976/1979 to 2008/2010 (km²) *(%)*
133	48°26.456′S, 73°40.706′W	G286342E48413S	A1, B12, C27, D37	5.51	–0.19 *(–3.31)*	–0.37 *(–4.21)*	–0.17 *(–4.72)*	–0.73 *(–12.77)*
134	48°24.121′S, 73°39.513′W	G286342E48413S	A1, B12, C27, D37	5.74	–0.46 *(–7.54)*	–0.40 *(–4.35)*	–0.10 *(–2.66)*	–0.96 *(–15.51)*
135	48°22.338′S, 73°40.183′W	G286342E48413S	A1, B12, C27, D42	9.63	NSC	NSC	–0.11 *(–1.41)*	–0.13 *(–1.34)*
136	48°20.552′S, 73°37.784′W	G286390E48352S	A6, B12, C27, D42	19.16	–0.10 *(–0.75)*	–0.34 *(–1.12)*	–0.16 *(–1.08)*	–0.61 *(–3.15)*
139	48°20.896′S, 73°29.284′W	Jorge Montt/ G286499E48466S	A1, B18, C27, D46	505.49	–2.45 *(–0.44)*	–41.48 *(–5.49)*	–9.82 *(–2.60)*	–53.75 *(–10.58)*
			Total (km²)	7613.54	–46.94	–156.27	–67.72	–272.70

*From 1984/1986 to 2008/2010.

at 2.29% decade^{-1}. This is reflected in the fact that 6 glaciers advanced during this period, 17 showed no significant change, and 55 retreated. This relatively slow rate of loss is matched by the eastern SPI during this interval, which recorded its lowest average basin retreat rate of 1.68% decade^{-1}.

Out of 78 glaciers measured between 2000/2002 and 2008/2010, 45 lost area and 2 gained area. This reflects the lowest proportion of retreating glaciers for any period, although the average retreat rate per basin was a little higher than the previous period at 2.44% decade^{-1} (Table 4). Overall, the west side of the icefield lost an area of 67.72 km^2 (0.89%). Similar to the long-term patterns, the largest absolute area losses occurred on large glaciers in the NW, such as the Jorge Montt (#139) which reduced in area by 9.82 km^2 (2.60% decade^{-1}). The highest relative area losses were also focused in this region, such as glacier #127, which retreated at a rate of 11.16% decade^{-1}. As with all periods, the highest rates of expansion were once again observed on the Pio XI (#117) and #115 glaciers, with increases of 0.48% and 1.79% decade^{-1}, respectively.

SPATIAL DISTRIBUTION OF GLACIER LOSSES

The spatial distribution of glacier changes across the SPI showed marked variability (Figs. 2, 3, and 6). From 1976/1979 to 1984/1986 the highest mean area losses occurred in the southeast (5.0% decade^{-1}), followed by the southwest (3.6% decade^{-1}) (Fig. 6, part a). During the period 1984/1986 to 2000/2002, mean area losses were dominated by the northwest (3.3% decade^{-1}) (Fig. 6, part b), while between 2000/2002 and 2008/2010, the highest shrinkage rates were found in both the northwest and southeast (3.2% decade^{-1}) (Fig. 6, part c). Over the entire study period, 1976/1979 to 2008/2010, the northwest had the highest mean shrinkage rates (2.9% decade^{-1}), while glaciers in the northeast had the lowest mean shrinkage rates (1.4% decade^{-1}).

Discussion

From the above results it is clear that losses have dominated glacier changes across the SPI since the 1970s, although the detailed patterns are variable over space and time. In terms of assessing the potential causes of these changes, we start below by assessing the relationships between area losses and physiography. After this, we review likely climatological influences, before comparing our findings to those of previous studies and assessing the causes of any major differences in reported patterns.

RELATIONSHIPS BETWEEN AREA LOSSES AND PHYSIOGRAPHY

A total of 10 terrain variables were derived for all 130 SPI basins measured in this study to determine the influence of physical location on observed area changes (Table 5). Spatial Analyst in ArcGIS 10.1 was used to calculate the minimum elevation, mean elevation, mean slope angle, and mean aspect for the glaciated portion of each basin from the SRTM DEM. To enable statistical analyses, the sine of the aspect was used to derive an east-west scalar aspect, and the cosine to derive a north-south scalar aspect (Copland, 1998). Glacier area, latitude, and longitude were taken from the existing data (Tables 2 and 3). Glacier centerline lengths were derived manually, using guidance provided by the SRTM DEM and surface features such as medial moraines. Finally, an index was created that numbered all glaciers as 1 if they terminated in water and 0 if they terminated on land.

There was strong collinearity between the terrain variables, so principal components analysis (PCA) was used to determine the relationships between them (Table 5). The PCA results were based on the correlation matrix between variables to standardize measurement units. PCA identified four significant components (eigenvalue >1), with component 1 representing a glacier size factor that indicates that large glaciers tend to have long centerline

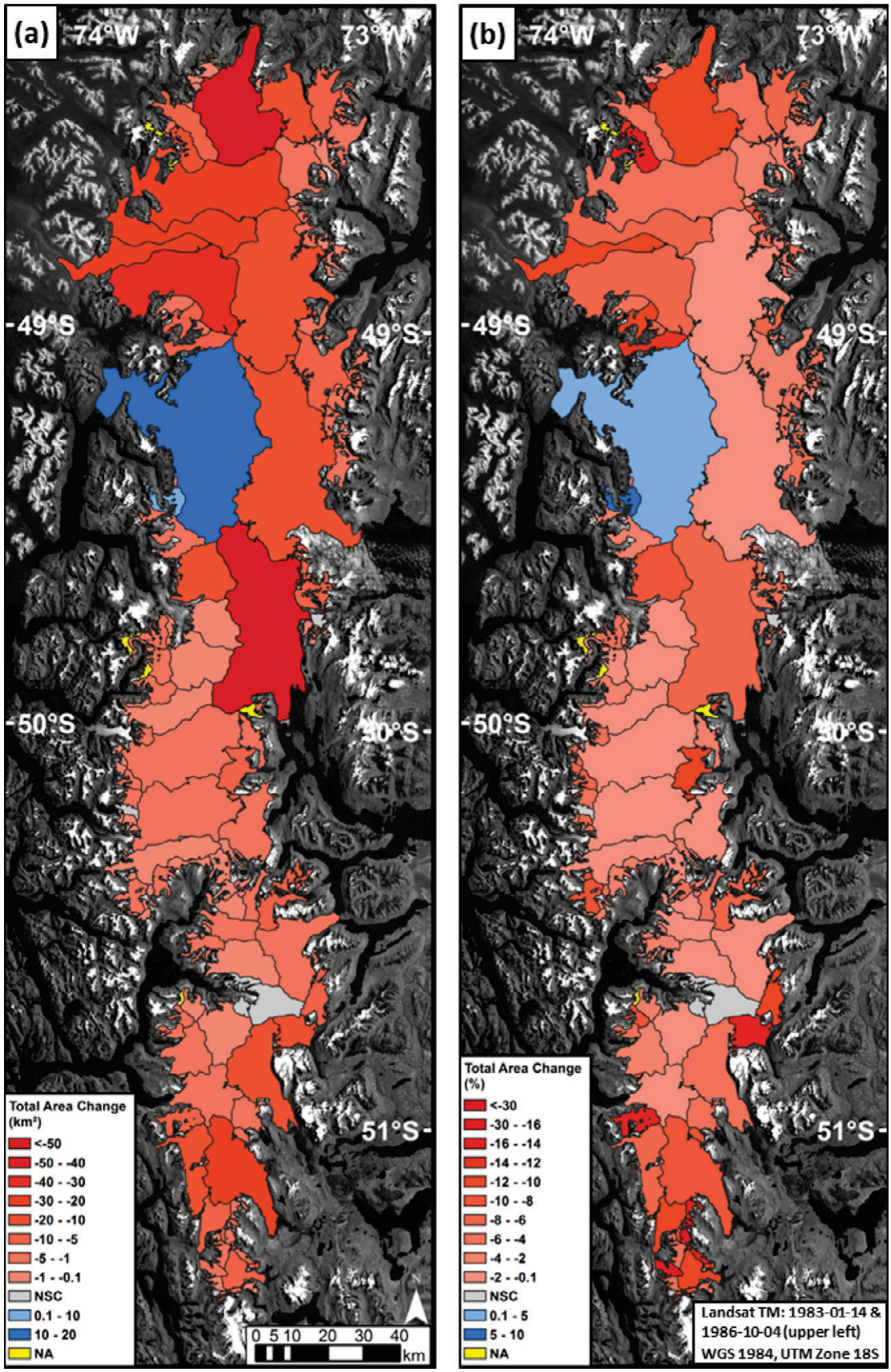

FIGURE 2. Area changes across the SPI over the longest measurement period (1976/1979 to 2008/2010 for 100 basins, 1984/1986 to 2008/2010 for 30 basins; see Tables 2 and 3 for details) in: (a) absolute values (km²); (b) relative values (%). NSC = no significant change beyond error limit of 0.1 km². NA = not applicable (not measured in this study).

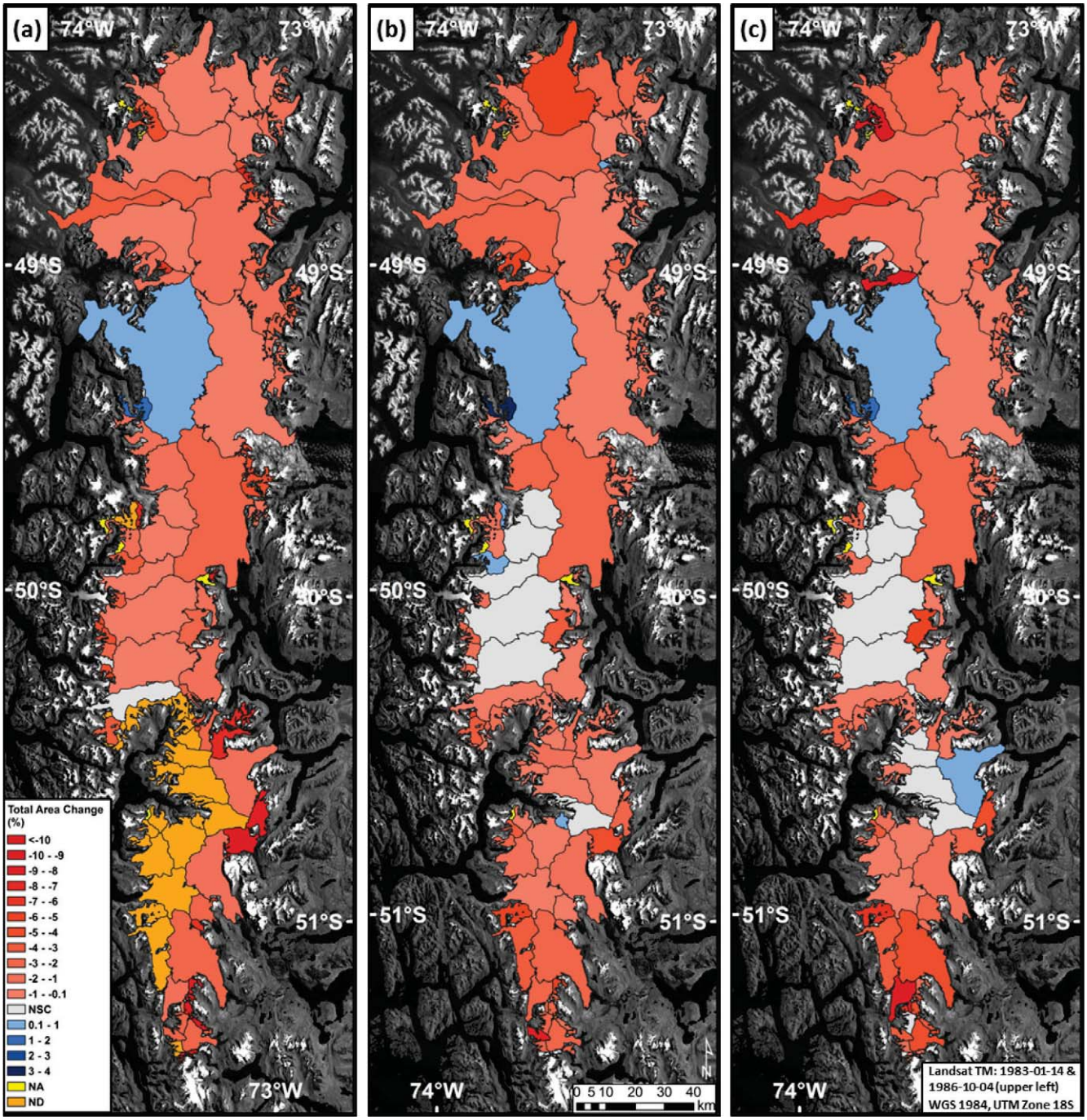

FIGURE 3. Area changes (% decade^{-1}) across the SPI broken down by measurement period: (a) 1976/1979 to 1984/1986; (b) 1984/1986 to 2000/2002; (c) 2000/2002 to 2008/2010. NSC = no significant change beyond error limit of 0.1 km^2. NA = not applicable (not measured in this study). ND = no data for that time period.

lengths, low average slope angles, and descend to low elevations. Component 2 is predominantly an east-west factor, which indicates that glaciers on the western side of the SPI tend to face west and have low mean elevations (likely due to the strong east-west precipitation gradient in this region). Component 3 is predominantly a north-south (latitude) factor, while component 4 describes how northerly or southerly the basin is facing. Vice versa conditions are also true for the above relationships.

The factor scores from the four significant principal components were correlated with the % decade^{-1} area changes recorded for each individual measurement period, as well as the longest measurement period (1984/1986 to 2008/2010) for which area changes from all basins were available (Table 6). Over the period 1976/1979 to 1984/1986 the first three components were all significantly correlated with the measured area changes; component 1 was the most important factor, which indicates that the biggest % decade^{-1} losses occurred on relatively short and small glaciers with steep surfaces and relatively high terminus elevations. Component 2 indicates that the biggest losses occurred on westerly glaciers with westerly aspects and relatively low mean elevations,

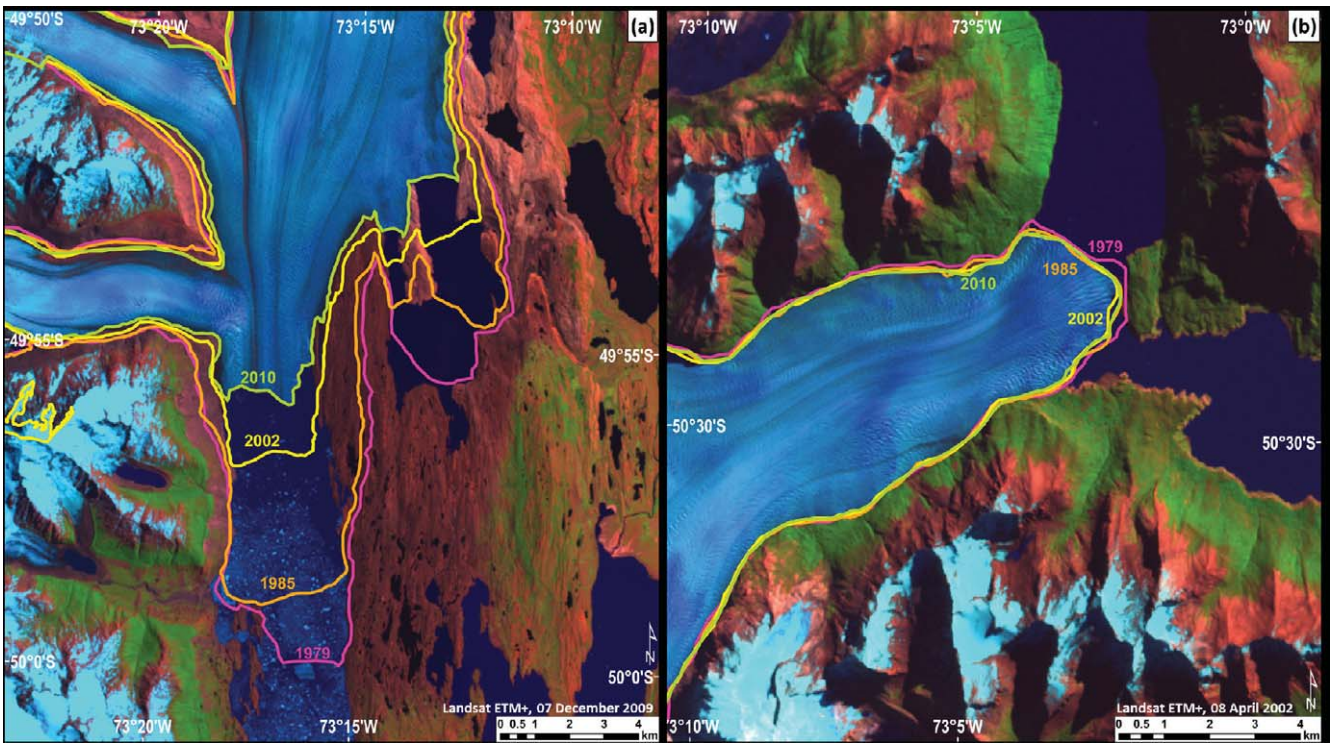

FIGURE 4. Area changes of the ablation zone of two glaciers on the eastern side of the SPI: (a) Upsala Glacier, ID # 29 (base image: Landsat ETM+, 7 Dec 2009); (b) Perito Moreno Glacier, ID # 40 (base image: Landsat ETM+, 8 Apr 2002).

while component 3 suggests that greater losses also occurred on glaciers with a more southerly location. In all of the other periods, only component 2 was significantly correlated with the measured area losses (Table 6), suggesting that only westerly location, westerly aspect, and low mean elevations were important during these times. When these component 2 terrain factors are individually plotted against area changes, however, it becomes clear that westerly location (Fig. 7, part a) and westerly aspect (Fig. 7, part b) are not significantly correlated with area changes, but mean elevation is strongly correlated (Fig. 7, part c; $p < 0.01$). Only the patterns for 1984/1986 to 2008/2010 are shown in Figure 7, but the patterns and correlations were very similar for the individual periods 1976/1979 to 1984/1986, 1984/1986 to 2000/2002, and 2000/2002 to 2008/2010. From these analyses, it is apparent that mean elevation provided the dominant topographic control on glacier shrinkage rates measured in this study,

TABLE 4

Summary of changes in glacier extent across the SPI.

	1976/1979 to 1984/1986	1984/1986 to 2000/2002	2000/2002 to 2008/2010	1976/1979 to 2008/2010
Eastern SPI (total km^2)	–74.51	–123.63	–70.64	–269.35
Western SPI (total km^2)	–46.94	–156.27	–67.72	–272.70
Total SPI (total km^2)	–121.45	–279.90	–138.36	–542.05
Eastern SPI (total %)[a]	–1.31	–2.18	–1.24	–4.74
Western SPI: (total %)[a]	–0.62	–2.05	–0.89	–3.58
Total SPI: (total %)[a]	–0.91	–2.11	–1.04	–4.08
Eastern SPI (per basin average; % decade^{-1})[b]	–3.44	–1.68	–2.00	–1.70
Western SPI (per basin average; % decade^{-1})[b]	–3.00	–2.29	–2.44	–2.29
Total SPI (per basin average; % decade^{-1})[b]	–3.24	–2.04	–2.24	–2.04

[a] Computed in relation to 1984/1986 total measured area (5677.81 km^2 eastern SPI + 7613.54 km^2 western SPI = 13291.35 km^2 total).
[b] Computed from average of % decade^{-1} changes measured per basin; these values are typically higher than the overall % changes, which are dominated by changes occurring in a few very large basins.

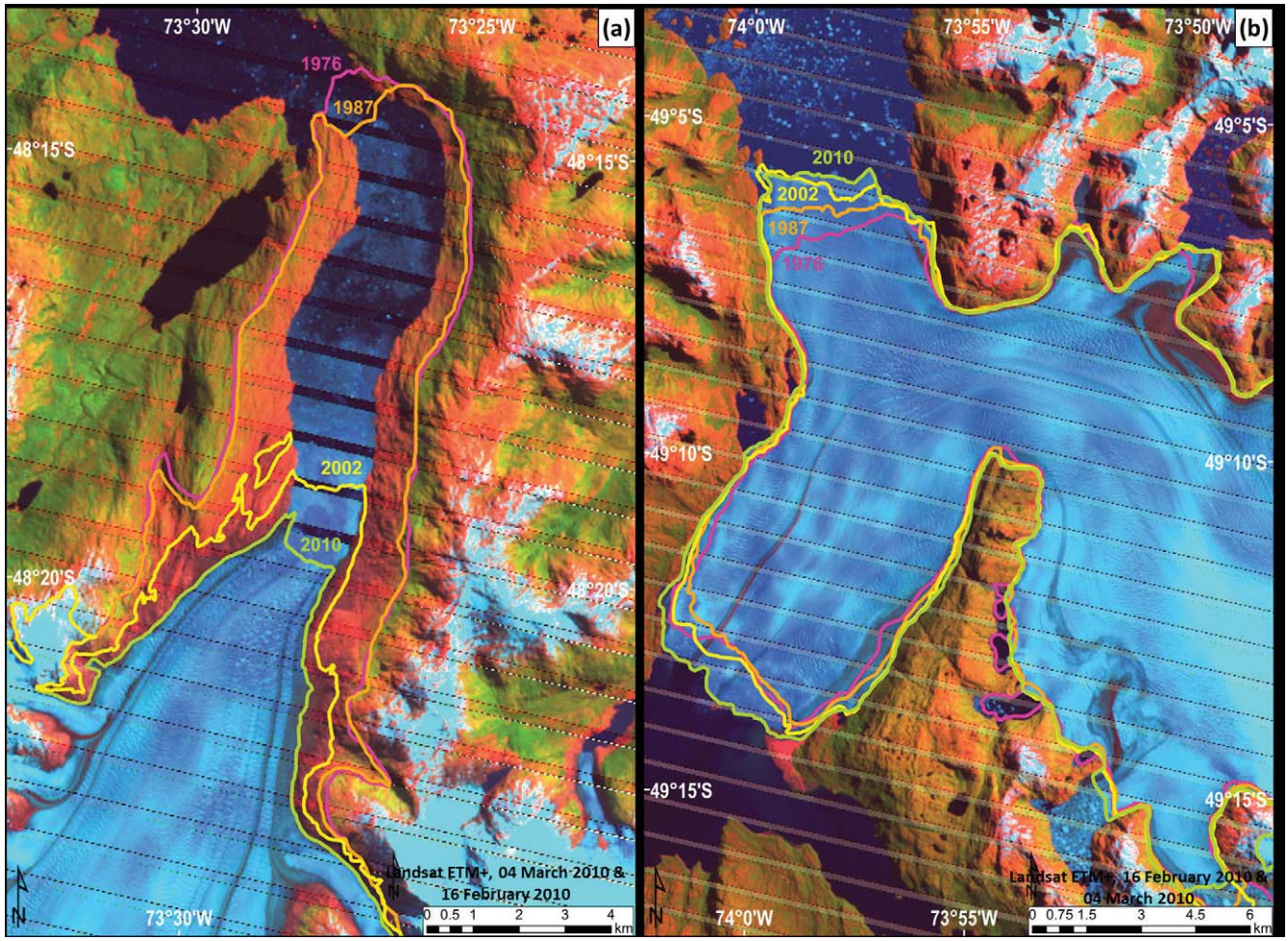

FIGURE 5. Area changes of the ablation zone of two glaciers with contrasting changes on the western side of the SPI: (a) Jorge Montt Glacier, ID # 139 (retreating); (b) Pio XI Glacier, ID# 117 (advancing). Base images are Landsat ETM+ from 16 Feb 2010 and 4 Mar 2010, combined to remove data gaps caused by failure of the scan-line corrector.

with highest shrinkage rates occurring at lower elevations. However, the one factor that has not been properly assessed yet is the effect of terminus environment (water- or land-terminating) on the observed area changes. This is because none of the four significant principal components showed a strong relationship to terminus environment (Table 5), so this influence is assessed separately below.

Previous measurements on water-terminating glaciers in Patagonia have shown that they are usually grounded, and are quasi-stable when in this configuration (Warren and Aniya, 1999). However, ice thinning can result in flotation of the terminus and a rapid increase in calving and retreat caused by the removal of back stress if a glacier retreats from a pinning point (e.g., island, terminal moraine). For example, the rapid recent retreat of Upsala Glacier (Fig. 4, part a) is likely related to a loss of terminus stability after it retreated past the Brazo Upsala islands (Skvarca et al., 2003). A comparison of our observed area changes over the period 1984/1986 to 2008/2010 with terminus environment and glacier size indicates that the shrinkage rate is more variable on marine-terminating glaciers than those terminating on land (Fig. 8). Over the same period, glaciers terminating in water had an average retreat rate of 1.78% decade^{-1}, while those terminating on land had an average retreat rate of 2.44% decade^{-1}. However, this may also be related to glacier size, as all large glaciers (>60 km^2) terminated in a marine environment, whereas most small glaciers (<10 km^2) are land-terminating (Fig. 8). This is consistent with the conclusion by Davies and Glasser (2012) that land-terminating glaciers have undergone higher relative losses than water-terminating glaciers.

CONNECTIONS WITH METEOROLOGICAL PATTERNS

In terms of climate, many studies have reported that atmospheric warming and decreases in precipitation have contributed to reductions in length, area, and thickness of SPI glaciers and surrounding regions in southern South America (e.g., Casassa, 1995; Rivera et al., 2002; Bown and Rivera, 2007; Rasmussen et al., 2007). For example, Rosenblüth et al. (1997) used meteorological station data from northern and southern Chile to determine a mean surface air temperature increase of 0.013 to 0.02 °C a^{-1} from 1933 to 1992, and double this amount from 1960 to 1992. The changes in temperature were not uniform across the study area, with cooling trends present in areas such as Puerto Montt. However, warming at the 850 hPa level (~1400 m eleva-

tion) has been consistently observed in several studies that used station National Centers for Environmental Prediction (NCEP)/National Center for Atmospheric Research (NCAR) reanalysis data to examine temperature changes between 1948 and 2000 (Karoly, 1987; Bown and Rivera, 2007; Rasmussen et al., 2007).

According to Giese et al. (2002), observations from the tropical Pacific Ocean show a post-1976 shift, leading to warmer than normal temperatures in the southern hemisphere. This shift seems apparent in studies examining recent trends in precipitation. Analysis of NCEP/NCAR reanalysis precipitation patterns across the SPI from 1960 to 1999 by Rasmussen et al. (2007) indicated little change in total precipitation amount since the 1950s, but a reduction in the snow-to-precipitation ratio that would result in a decrease in annual snow accumulation and an increase in energy for melt from rain on the glacier surface. Bown and Rivera (2007) did identify a decreasing precipitation trend in station data (located between 38°S and 42°S) from 1950 to 2000, particularly in the 1980s and 1990s. They argued that increasing temperature and decreasing precipitation has likely caused a decrease in snowfall and an increase in ablation leading to the increasing elevation of the equilibrium line altitude (Bown and Rivera, 2007).

According to Carrasco et al. (2000) the spatial distribution of precipitation changes has varied across southern South America. Meteorological data from the Cabo Raper and San Pedro stations (both located to the northwest of the SPI) (Rivera et al., 2002) have shown decreasing precipitation trends since the 1980s, while the Lord Cochrane and Lago Argentino stations (located to the northeast of the SPI) have shown increasing precipitation trends since the 1980s (Karoly, 1987; Carrasco et al., 2002). If these precipitation observations are applied to the respective quadrants of the SPI, their trends are in line with the overall glacier changes recorded in this study, with highest shrinkage in the northwest versus smaller changes in the northeast (Fig. 6). In the south-

TABLE 5

Explained variance for each significant component (eigenvalue > 1) identified in principal components analysis. + or – indicates whether relationship between terrain parameter and component is positive or negative. Bold indicates dominant terrain parameter(s) for each principal component.

Principal component	1	2	3	4
Latitude	+0.00%	+22.30%	**+52.75%**	+0.05%
Longitude	+18.10%	**+55.56%**	–11.10%	+0.02%
Minimum elevation	**–52.88%**	–10.44%	–9.43%	–8.30%
Mean elevation	–2.88%	**–55.24%**	–3.00%	+0.02%
Mean slope	**–69.62%**	+1.77%	+0.16%	+5.90%
Centerline length	**+76.25%**	–13.27%	–0.45%	–0.36%
Area	**+55.40%**	–17.43%	–1.05%	–0.64%
East-west aspect	–12.40%	**–41.68%**	+17.20%	+0.32%
North-south aspect	–0.51%	–0.03%	–10.66%	**+77.39%**
Land or water terminus	+22.41%	–12.85%	+13.80%	+15.05%
Eigenvalue (out of 10)	3.10	2.31	1.20	1.08

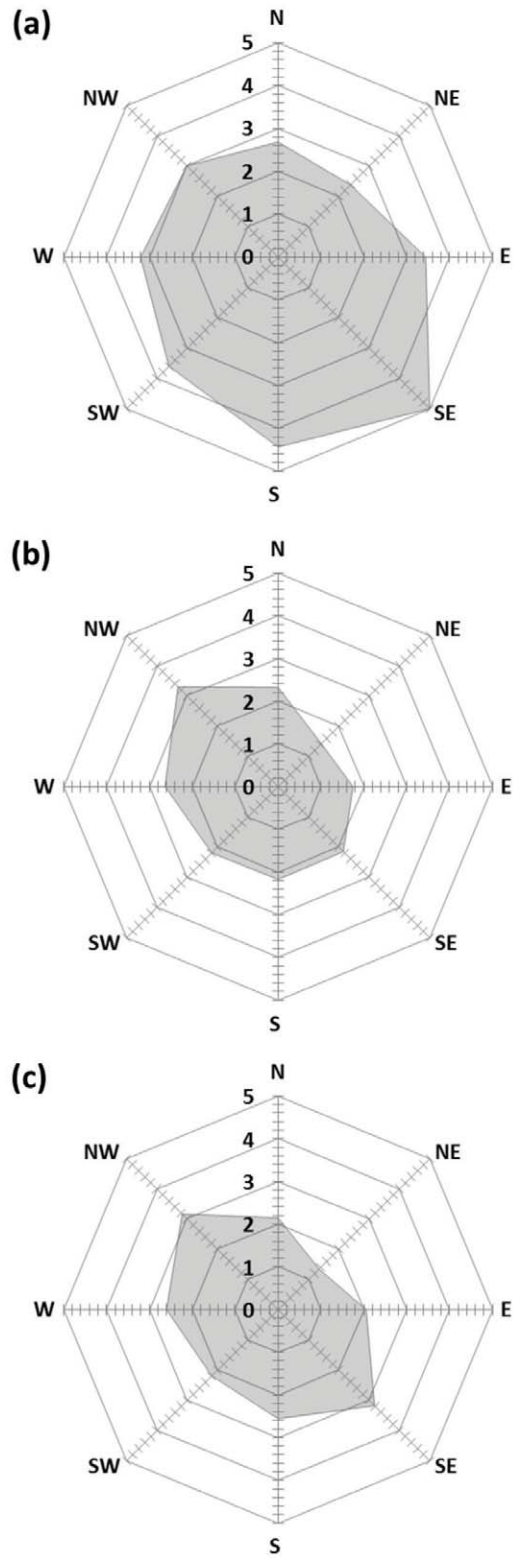

FIGURE 6. Radar graphs illustrating the distribution of mean annual shrinkage rates (% decade^{-1}) by location and study period: (a) 1976/1979 to 1984/1986; (b) 1984/1986 to 2000/2002; (c) 2000/2002 to 2008/2010. Note that glaciers which expanded are not included in this figure.

TABLE 6

Pearson's correlation coefficient (r) between the four significant principal components and % decade^{1} area changes recorded at every glacier basin across the SPI. Correlations significant at 95% level are highlighted in bold.

Principal component	1	2	3	4
1976/1979 to 1984/1986 area change (% decade^{-1})	**0.404**	**–0.300**	**–0.253**	0.016
1984/1986 to 2000/2002 area change (% decade^{-1})	0.130	**–0.247**	0.146	0.108
2000/2002 to 2008/2010 area change (% decade^{-1})	0.004	**–0.272**	–0.047	–0.004
1984/1986 to 2008/2010 area change (% decade^{-1})	0.092	**–0.237**	0.088	0.030

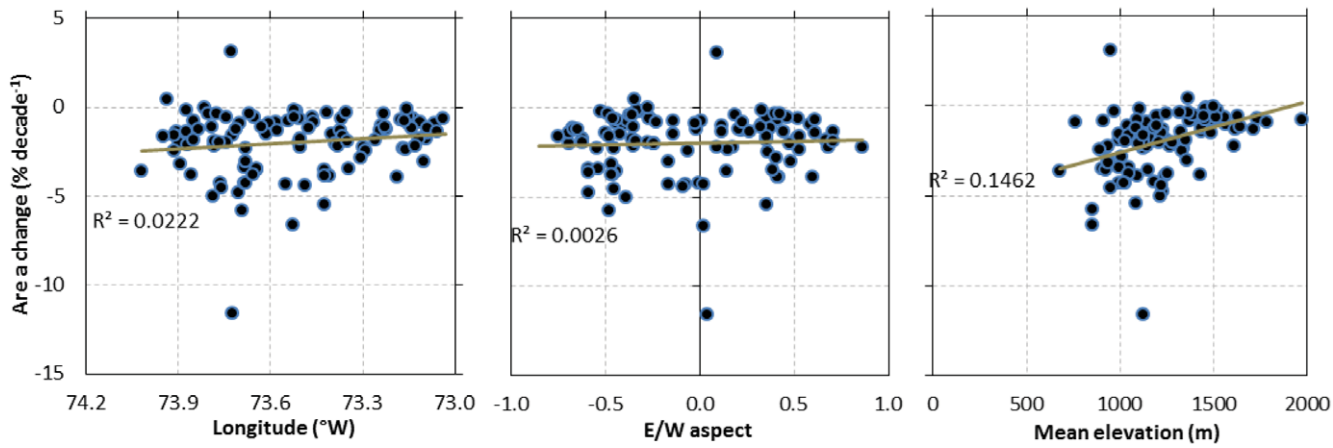

FIGURE 7. Comparison between 1984/1986 and 2008/2010 area changes for 130 measured glaciers and: (a) longitude; (b) E/W aspect; and (c) mean elevation. Line indicates best-fit linear trendline.

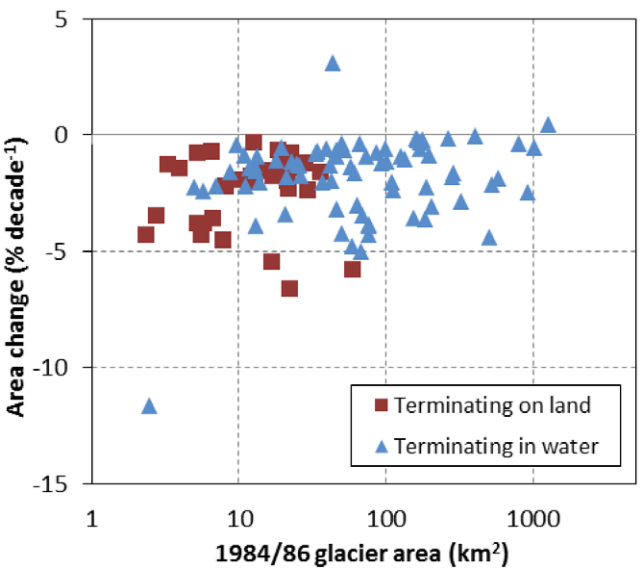

FIGURE 8. Relationship between glacier area and area change between 1984/1986 and 2008/2010 for all 130 measured basins, classified by terminus environment. Note log scale on x-axis.

ern SPI, the nearest station to the southwest quadrant is located 150 km away at Faro Evangelista (52°24′S, 75°36′W) where precipitation has been increasing since 1983, while meteorological data from the Rio Gallegos station (51°37′S, 69°17′W), located to the southeast of the SPI, demonstrated a decreasing precipitation trend from 1927 to 1990 (Carrasco et al., 2002; Ibarzabal y Donángelo et al., 1996). Once again, these trends correspond with the changes observed in this study where glacier losses have been generally lower in the southwest than the southeast (Fig. 6).

COMPARISON WITH PREVIOUS STUDIES

Over the 1940s–1990s, Aniya et al. (1997) and Aniya (1999) reported higher retreat rates in the north of the SPI compared to the south, with glaciers north of 50°S having the greatest retreat rates (0.126 km^2 a^{-1}), particularly in the northwest (0.110 km^2 a^{-1}). Their lowest retreat rates were in the south (0.083 km^2 a^{-1}), with the southwest experiencing the lowest retreat rate of <0.020 km^2 a^{-1}. Over the period 1968/1975–2000, Rignot et al. (2003) similarly recorded that glaciers on the northern half thinned more rapidly than glaciers on the southern half. When assessed in terms of absolute area changes, our study supports a similar north-south differentiation over the period 1984/1986 to 2008/2010, with glaciers in the north losing absolute area at a substantially higher rate (0.27 km^2 a^{-1}) than glaciers in the south (0.10 km^2 a^{-1}), and greatest retreat rates in the northwest and lowest in the southwest. The story appears somewhat different when expressed in terms of relative area changes, however, with little difference in losses between the north (2.1% decade^{-1}) and south (2.0% decade^{-1}) over the period 1984/1986 to 2008/2010. This illustrates the caution that must be

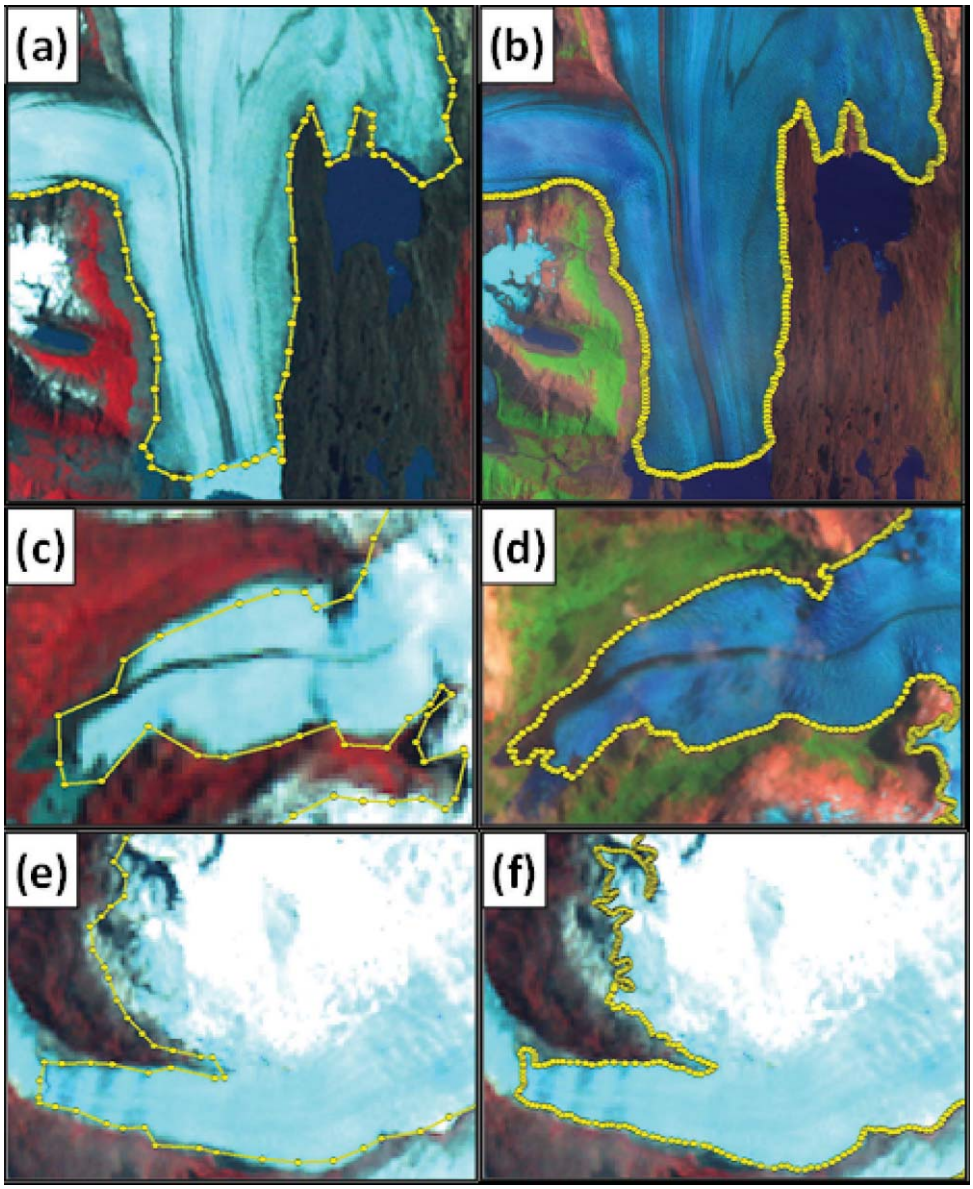

FIGURE 9. Comparison between: (a, c, e) glacier outlines produced by Davies and Glasser (2012), downloaded from the GLIMS online database (http://glims.colorado.edu/cgi-bin/mapserv), and (b, d, f) those completed for this study. The glaciers were selected at random and include (a, b) Upsala (ID #29); (c, d) ID #86; (e, f) HPS12 (ID #113), overlain on the satellite image used to produce each outline: (a, c, e, f) Landsat 5 MSS, 14 January 1986; (b, d) Landsat TM, 27 January 1985.

made when comparing previous studies of the SPI, with some studies expressing their change values in units of $km^2\ a^{-1}$ (e.g., Aniya et al., 1997; Aniya, 1999), and others expressing their changes in units of $\%\ a^{-1}$ (e.g., Davies and Glasser, 2012). To help with this issue, we have expressed all of our area changes in both units.

The picture of long-term losses of the SPI determined in this study are consistent with earlier work, although some of the details differ from the findings of Davies and Glasser (2012). For example, they reported an area loss of 233.3 km^2 between 1986 and 2001, compared to our calculations of a 279.9 km^2 loss over the period 1984/1986 to 2000/2002 (Table 4). Between 2000/2002 and 2008/2010 our study recorded an area loss of 138.4 km^2, compared to the 205.2 km^2 recorded by Davies and Glasser (2012). To investigate the reasons for these differences, we downloaded the outlines produced by Davies and Glasser (2012) from the GLIMS database and compared them with our own. We found that the Davies and Glasser outlines were consistently defined by far fewer points than ours, and also missed details of glacier margins that we mapped (Fig. 9). Combined with methodological differences (e.g., whether interior nunataks were included in the calculations), differences in the identification of glacier outlines by different operators (Paul et al., 2013), slightly different ranges in the years of study for each period, and the inclusion of small peripheral glaciers in the inventory of Davies and Glasser (2012), this likely explains the differences between our results.

In our study only two glaciers, the Pio XI (#117) and adjacent #115, showed long-term area increases (Figs. 2 and 5, part b; Table 3). The looped moraines visible on the Pio XI terminus in satellite imagery suggest that this increase has likely been due to surging (Meier and Post, 1969). Rivera et al. (1997a, 1997b) proposed several explanations for this surging, including increased sliding caused by geothermal activity, enhanced basal water pressure, increased precipitation prior to surge events, and reduced calving as water depths decreased at the glacier front from sedimentation. It is therefore likely that the expansion of these glaciers was dominated by changes in internal dynamics, rather than the changes in climate that appear to dominate the losses recorded at almost all of the glaciers measured in this study.

Conclusions

Of the glaciers measured across the SPI in this study, the vast majority have decreased in area since the 1970s. Loss rates were greatest over the period 1976/1979 to 1984/1986, with 87% of measured glaciers showing significant losses at an average rate of 3.24% decade^{-1}. This compares to 75% of glaciers losing area between 1984/1986 and 2000/2002 (at 2.04% decade^{-1}), and 64% of glaciers losing area between 2000/2002 and 2008/2010 (at 2.24% decade^{-1}). Assigning the causes of glacier losses in Patagonia is difficult given the complex interplay between physiography, tidewater glacier dynamics, variability in response times between glaciers of different sizes, climate, and other factors such as debris. Based on our analysis, mean glacier elevation provided the only consistent topographic control on glacier changes across all measurement periods, with greatest losses at lower elevations. Loss rates also appear to be greatest on land-terminating glaciers, although the variability in loss rates is greater on water-terminating glaciers. The paucity of long-term climate data from stations adjacent to the SPI makes detailed climate analysis difficult, but the general pattern of losses is consistent with regional warming of up to 0.4 °C decade^{-1} between 1960 and 1992, which has resulted in a lengthened melt season and reduction in the proportion of total precipitation falling as snow (Rosenblüth et al., 1997; Bown and Rivera, 2007). Spatial variability in precipitation rates also appear to be consistent with spatial variability in glacier retreat rates, with the largest retreat rates corresponding with the greatest decreases in precipitation in the NW of the SPI.

To improve understanding of the connections between climate and changes in glacier area, an improved network of weather stations and mass balance monitoring locations needs to be installed across the SPI. Further investigations, such as detailed bathymetric surveys at glacier fronts, also need to be completed to investigate why some glaciers have displayed extremely high losses (e.g., Upsala), while others nearby have remained stationary or even advanced. Additional factors such as the development of proglacial lakes, underlying topography, and the presence of debris cover can have a strong influence on glaciers, and therefore further investigation of these are required to better understand the ice losses observed across the SPI.

Acknowledgments

We thank Canada Foundation for Innovation, Ontario Research Fund, Natural Resources and Engineering Research Council of Canada, University of Ottawa, and Natural Resources Canada for assistance with funding. We also thank the members of the Laboratory for Cryospheric Research for their support, Francisca Bown for providing shapefiles of the 1986 and 2001 basin boundaries for the SPI, and Derek Mueller for helpful reviews. We appreciate comments provided by two anonymous reviewers.

References Cited

Aniya, M., 1999: Recent glacier variations of the Hielos Patagónicos, South America, and their contribution to sea-level change. *Arctic, Antarctic, and Alpine Research,* 31: 165–173.

Aniya, M., Naruse, R., Shizukuishi, M., Skvarca, P., and Casassa, G., 1992: Monitoring recent glacier variations in the Southern Patagonia Icefield, utilizing remote sensing data. *International Archives of Photogrammetry and Remote Sensing,* 29: 87–94.

Aniya, M., Sato, H., Naruse, R., Skvarca, P., and Casassa, G., 1996: The use of satellite and airborne imagery to inventory outlet glaciers of the Southern Patagonia Icefield.*Photogrammetric Engineering and Remote Sensing,* 62: 1361–1369.

Aniya, M., Sato, H., Naruse, R., Skvarca, P., and Casassa, G., 1997: Recent glacier variations in the Southern Patagonia Icefield, South America. *Arctic and Alpine Research,* 29: 1–12.

Bown, F., and Rivera, A., 2007: Climate changes and recent glacier behavior in the Chilean Lake District. *Global and Planetary Change,* 59: 79–86.

Carrasco, J., Casassa, G., and Rivera, A., 2002: Meteorological and climatological aspects of the Southern Patagonia Ice Cap, Patagonia. *In* Casassa, G., Sepúlveda, F., Sinclair, R. (eds.), *The Patagonian Icefields. A Unique Laboratory for Environmental and Climate Change Studies.* New York: Kluwer Academic/Plenum Publishers, 29–41.

Casassa, G., 1992: Radio-echo sounding of Tyndall Glacier, southern Patagonia. *Bulletin of Glacier Research,* 10: 69–74.

Casassa, G., 1995: Glacier inventory in Chile: current status and recent glacier variations. *Annals of Glaciology,* 21: 317–322.

Chaltén Out Door Maps, 2010: Glacier Perito Moreno topographical map El Calafate. El Chaltén, Argentina: Chaltén Out Door Maps, 1:90,000.

Chen, J. L., Wilson, C. R., Tapley, B. D., Blankenship, D. D., and Ivins, E. R., 2007: Patagonia Icefield melting observed by Gravity Recovery and Climate Experiment (GRACE). *Geophysical Research Letters,* 34: 6 pp., http://dx.doi.org/10.1029/2007GL031871.

Copland, L., 1998: The use of terrain analysis in the evaluation of snow cover over an alpine glacier. *In* Lane, S. N., Richards, K. S., and Chandler, J. H. (eds.), *Landform Monitoring, Modelling and Analysis.* Chichester, UK: John Wiley & Sons, 385–404.

Davies, B. J., and Glasser, N. F., 2012: Accelerating shrinkage of Patagonian glaciers from the Little Ice Age (~AD 1870) to 2011. *Journal of Glaciology,* 58: 1063–1084.

Giese, B. S., Urizar, S. C. and Fučkar, N. S., 2002: Southern hemisphere origins of the 1976 climate shift. *Geophysical Research Letters,* 29: 4 pp., http://dx.doi.org/10.1029/2001GL013268.

Glasser, N. F., and Gudmundsson,G. H., 2012: Longitudinal surface structures (flowstripes) on Antarctic glaciers. *The Cryosphere,* 6: 383–391.

Hall, D. K., Baa, K. J., Schöner, W., Bindschadler, R. A., and Chien, J. Y. L., 2003: Consideration of the errors inherent in mapping historical glacier positions in Austria from the ground and space (1893–2001). *Remote Sensing of Environment,* 86: 566–577.

Ibarzabal y Donángelo, T., Hoffmann, J. A., and Naruse, R., 1996: Recent climate changes in southern Patagonia. *Bulletin of Glacier Research,* 14: 29–36.

Jacob, T., Wahr, J., Pfeffer, W., and Swenson, S., 2012: Recent contributions of glaciers and ice caps to sea level rise. *Nature,* 482: 514–518.

Karoly, D. J., 1987: Southern hemisphere temperature trends: a possible greenhouse effect? *Geophysical Research Letters*, 14: 1139-1141.

López, P., Chevallier, P., Favier, V., Pouyaud, B., Ordenes, F., and Oerlemans, J., 2010: A regional view of fluctuations in glacier length in southern South America. *Global and Planetary Change,* 71: 85–108.

Meier, M. F., and Post, A. S., 1969: What are glacier surges? *Canadian Journal of Earth Sciences,* 6: 807–817.

Nichols, R. L., and Miller, M. M., 1952: The Moreno Glacier, Lago Argentino, Patagonia: advancing glaciers and nearby simultaneously retreating glacier. *Journal of Glaciology,* 2: 41–46.

Paul, F., and 19 others, 2013: On the accuracy of glacier outlines derived from remote-sensing data. *Annals of Glaciology,* 54(63): 171–182.

Rasmussen, L., Conway, H., and Raymond, C., 2007: Influence of upper air conditions on the Patagonian Icefields. *Global and Planetary Change,* 59: 203–216.

Raup, B., and Khalsa, S. J. S., 2010: *GLIMS Analysis Tutorial*. Boulder, Colorado: National Snow and Ice Data Center, www.glims.org/MapsAndDocs/assets/GLIMS_Analysis_Tutorial_a4.pdf (accessed 16 April 2013).

Rignot, E., Rivera, A., and Casassa, G., 2003: Contribution of the Patagonia Icefields of South America to sea level rise. *Science,* 302: 434–437.

Rivera, A., 2004: *Mass Balance Investigations at Glaciar Chico, Southern Patagonia Icefield, Chile.* Ph.D. thesis, School of Geographical Sciences, University of Bristol, U.K., 303 pp.

Rivera, A., and Casassa, G., 2004: Ice elevation, areal, and frontal changes of glaciers from National Park Torres del Paine, Southern Patagonia Icefield. *Arctic, Antarctic, and Alpine Research,* 36: 379–389.

Rivera, A., Aravena, J. C., and Casassa, G., 1997a: Recent fluctuations of Glaciar Pio XI, Patagonia: Discussion of glacial surge hypothesis. *Mountain Research and Development,* 17: 309–322.

Rivera, A., Lange, H., Aravena, J. C., and Casassa, G., 1997b: The 20th-century advance of Glaciar Pio XI, Chilean Patagonia. *Annals of Glaciology,* 24: 66–71.

Rivera, A., Acuña, C., Casassa, G., and Bown, F., 2002: Use of remotely sensed and field data to estimate the contribution of Chilean glaciers to eustatic sea-level rise. *Annals of Glaciology*, 34: 367-372.

Rivera, A., Casassa, G., Bamber, J., and Kääb, A., 2005: Ice elevation changes of Glaciar Chico, southern Patagonia, using ASTER DEMs, aerial photographs and GPS data. *Journal of Glaciology,* 51: 105–112.

Rosenblüth, B., Fuenzalida, H. A., and Aceituno, P. , 1997: Recent temperature variations in Southern South America. *International Journal of Climatology,* 17: 67–85.

Skvarca, P., Raup, B., and De Angelis, H., 2003: Recent behaviour of Glaciar Upsala, a fast-flowing calving glacier in Lago Argentino, southern Patagonia. *Annals of Glaciology,* 36: 184–188.

Warren, C. R., 1994: Freshwater calving and anomalous glacier oscillations: recent behavior of Moreno and Ameghino glaciers, Patagonia. *Holocene,* 4: 422–429.

Warren, C., and Aniya, A., 1999: The calving glaciers of southern South America. *Global Planetary Change,* 22: 59–77.

Warren, C. R., and Rivera, A., 1994: Non-linear response of calving glaciers: a case study of Pio XI Glacier. *Revista Chilena de Historia Natural,* 67: 385–394.

Warren, C. R., Greene, D. R., and Glasser, N. F., 1995: Upsala Glacier, Patagonia: rapid calving retreat in freshwater. *Annals of Glaciology,* 21: 311–316.

Williams, R. S., Jr., Hall, D. K., Sigurdsson, O., and Chien, J. Y. L., 1997: Comparison of satellite-derived with ground-based measurements of the fluctuations of the margins of Vatnajökull, Iceland, 1973–92. *Annals of Glaciology,* 24: 72–80.

Willis, M. J., Melkonian, A. K., Pritchard, M. E., and Rivera, A., 2012: Ice loss from the Southern Patagonian Ice Field, South America, between 2000 and 2012. *Geophysical Research Letters,* 39: L17501, http://dx.doi.org/10.1029/2012GL053136.

Zagier and Urruty, 2010: Patagonian South Icefield trekking map. Buenos Aires: Zagier and Urruty Publications.

MS accepted September 2014